Cell Reports

Article

A pre-vaccination immune metabolic interplay determines the protective antibody response to a dengue virus vaccine

Graphical abstract

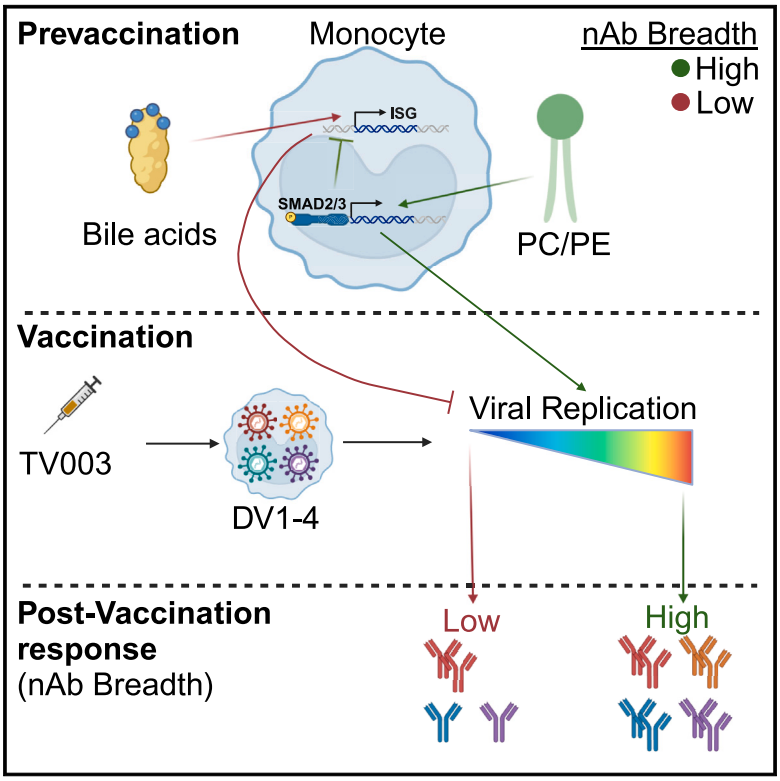

Authors

Adam-Nicolas Pelletier, Gabriela Pacheco Sanchez, Abdullah Izmirly, ..., Elias K. Haddad, Esper G. Kallas, Rafick Pierre Sekaly

Correspondence

rafick.sekaly@emory.edu

In brief

Pelletier et al. perform a systems immunology study of the pre-vaccination determinants of the dengue vaccine Butantan-TV003 humoral response. They show that metabolites PC/PE and bile acids, respectively, induce an anti- and a pro-inflammatory signature in monocytes. This immunometabolic crosstalk is associated with variability in the breadth of the neutralizing antibody response.

Highlights

- Phosphatidylcholine/phosphatidylethanolamine (PC/PE) induce TGF-β signaling in monocytes
- Bile acids (BAs) induce type I IFN in monocytes
- Efficacy of dengue vaccine Butantan-TV003 requires a broad nAb response to all four serotypes
- nAb response to Butantan-TV003 is associated with pre-vaccination levels of BAs and PC/PE

Pelletier et al., 2024, Cell Reports *43*, 114370
July 23, 2024
https://doi.org/10.1016/j.celrep.2024.114370

CellPress

Cell Reports

CellPress
OPEN ACCESS

Article

A pre-vaccination immune metabolic interplay determines the protective antibody response to a dengue virus vaccine

Adam-Nicolas Pelletier,[1,2] Gabriela Pacheco Sanchez,[3] Abdullah Izmirly,[4] Mark Watson,[5] Tiziana Di Pucchio,[3] Karina Inacio Carvalho,[2,6] Abdelali Filali-Mouhim,[7] Eustache Paramithiotis,[5] Maria do Carmo S.T. Timenetsky,[8] Alexander Roberto Precioso,[9] Jorge Kalil,[10,11] Michael S. Diamond,[12] Elias K. Haddad,[13] Esper G. Kallas,[9,14] and Rafick Pierre Sekaly[3,15,*]

[1]RPM Bioinfo Solutions, Sainte-Thérèse, QC, Canada
[2]Department of Pathology, Case Western Reserve University School of Medicine, Cleveland, OH, USA
[3]Pathology Advanced Translational Research Unit, Department of Pathology and Laboratory Medicine, Emory University School of Medicine, Atlanta, GA, USA
[4]Department of Medical Laboratory Sciences, Faculty of Applied Medical Sciences, King Abdulaziz University, Jeddah, Saudi Arabia
[5]CellCarta, Montreal, QC, Canada
[6]Hospital Israelita Albert Einstein, São Paulo, SP, Brazil
[7]Centre de recherche du Centre hospitalier de l'Université de Montréal (CRCHUM), Montreal, QC, Canada
[8]Instituto Adolfo Lutz, São Paulo, Brazil
[9]Instituto Butantan, São Paulo, Brazil
[10]Laboratory of Immunology, Heart Institute (InCor), Hospital das Clínicas da Faculdade de Medicina da Universidade de São Paulo (HCFMUSP), São Paulo, SP, Brazil
[11]Institute for Investigation in Immunology-Instituto Nacional de Ciência e Tecnologia-iii-INCT, São Paulo, SP, Brazil
[12]Departments of Medicine, Molecular Microbiology, and Pathology & Immunology, Washington University School of Medicine, St. Louis, MO 63110, USA
[13]Department of Medicine and Microbiology and Immunology, Drexel University College of Medicine, Philadelphia, PA, USA
[14]Department of Infectious and Parasitic Diseases, Hospital das Clínicas, School of Medicine, University of Sao Paulo, São Paulo 01246-903, Brazil
[15]Lead contact
*Correspondence: rafick.sekaly@emory.edu
https://doi.org/10.1016/j.celrep.2024.114370

SUMMARY

Protective immunity to dengue virus (DENV) requires antibody response to all four serotypes. Systems vaccinology identifies a multi-OMICs pre-vaccination signature and mechanisms predictive of broad antibody responses after immunization with a tetravalent live attenuated DENV vaccine candidate (Butantan-DV/TV003). Anti-inflammatory pathways, including TGF-β signaling expressed by $CD68^{low}$ monocytes, and the metabolites phosphatidylcholine (PC) and phosphatidylethanolamine (PE) positively correlate with broadly neutralizing antibody responses against DENV. In contrast, expression of pro-inflammatory pathways and cytokines (IFN and IL-1) in $CD68^{hi}$ monocytes and primary and secondary bile acids negatively correlates with broad DENV-specific antibody responses. Induction of TGF-β and IFNs is done respectively by PC/PE and bile acids in $CD68^{low}$ and $CD68^{hi}$ monocytes. The inhibition of viral sensing by PC/PE-induced TGF-β is confirmed *in vitro*. Our studies show that the balance between metabolites and the pro- or anti-inflammatory state of innate immune cells drives broad and protective B cell response to a live attenuated dengue vaccine.

INTRODUCTION

Dengue infection is a mosquito-transmitted viral disease caused by one of the four serotypes of dengue viruses (DENV-1, -2, -3, and -4). This disease is endemic in more than 100 countries, mainly in tropical and subtropical regions, with the highest incidence of infection in southeast Asia and South and Central America.[1] Clinical manifestations of dengue infection range from an asymptomatic or mild disease to severe dengue, a life-threatening vascular leakage syndrome associated with cytokine storm[2] and multiorgan failure.[3] While each DENV serotype can cause severe disease after primary infection, a secondary infection with a heterologous DENV serotype has been associated with an increased risk of severe dengue. This epidemiological pattern has been linked to antibody (Ab)-dependent enhancement (ADE) of infection[4,5]; in ADE, cross-reactive, poorly neutralizing Abs from the first infection facilitate the secondary infection by increasing the uptake of DENV virions in myeloid cells via interactions with Fc-γ receptors.[6,7]

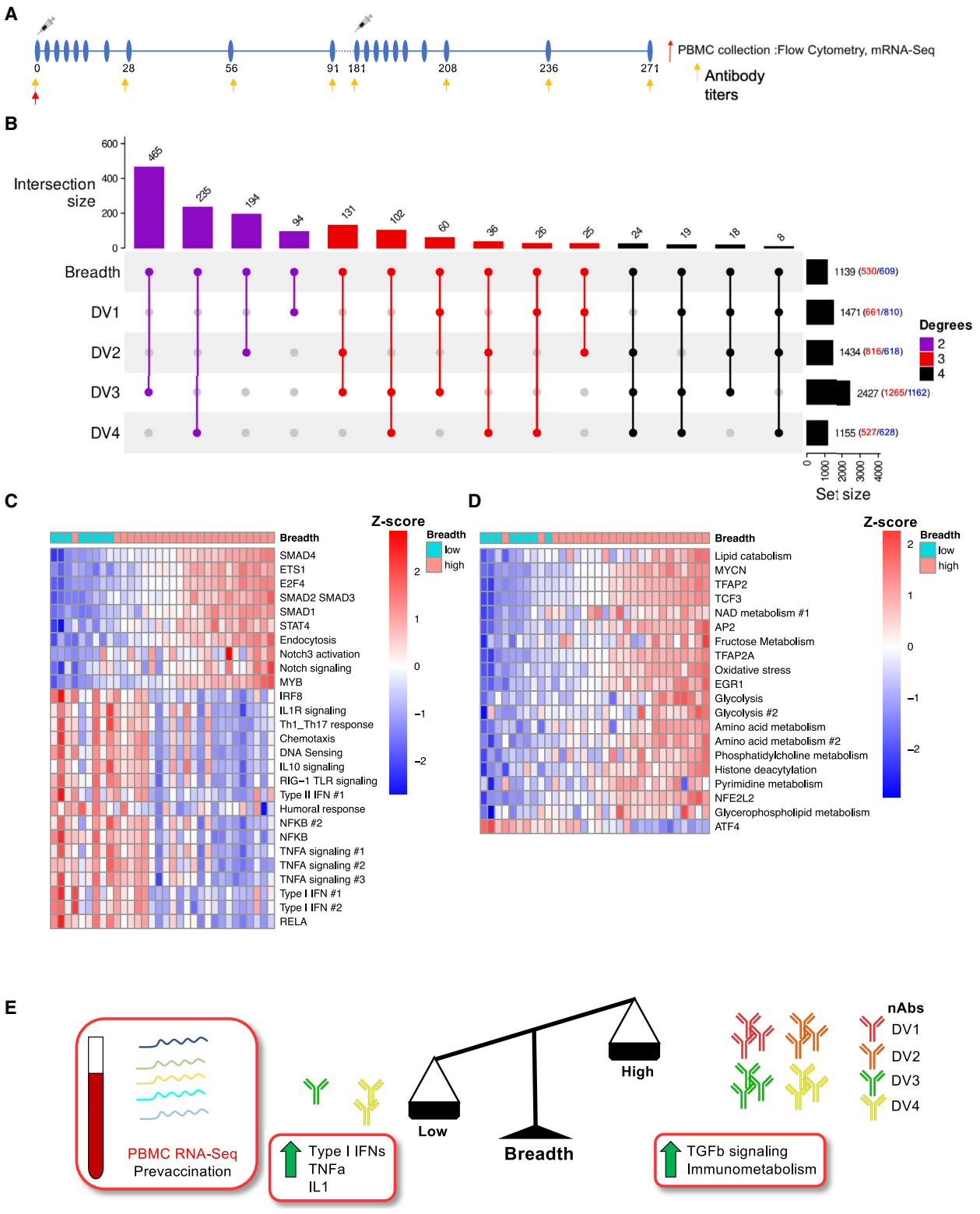

Figure 1. PBMC transcriptomic analysis of pre-vaccination of Butantan-DV/TV-003 vaccine-induced breadth of the neutralizing response reveals a dichotomic association of pro- versus anti-inflammatory pathways

(A) Design of phase II Butantan-DV/TV-003 clinical trial in naive subjects, with one primary injection at day 0 and a second dose at day 180. PBMCs were collected at days 0, 6, and 15, and plasma was collected at day 0.

(legend continued on next page)

The first authorized vaccine against DENV, the live attenuated Dengvaxia (CYD-TDV), was approved in dengue-endemic countries throughout Asia and Central/South America in 2016, with an efficacy that differed by serotype and by age group.[8] The largest benefits were found in children with a positive pre-vaccination serostatus, whereas vaccinated seronegative children (<9 years of age) were later shown to have an increased likelihood of hospitalization.[9,10] This result has been suggested to be caused by ADE in a manner similar to secondary DENV infection.[11,12] This has led the field to define a protective vaccine-induced immune response by seropositivity to all four serotypes.[11] Several other vaccine platforms (chimeric live attenuated viruses, inactivated plus AS04 adjuvant, DNA vaccine plus VAXFECTIN adjuvant, and recombinant proteins) are currently in human clinical trials, including TAK-003 (chimeric live attenuated virus); this vaccine triggered tetravalent neutralizing Ab (nAb) and cellular immune responses.[13–15] The TAK-003 vaccine showed a 3-year efficacy of 54.3% against DENV infection and 77.1% against hospitalization in pre-vaccination seronegative participants.[16] The contribution of innate immunity and the host environment to the heterogeneity observed in vaccine-mediated protection has not been addressed in these DENV vaccine trials.

The heterogeneity of the magnitude and durability of the immune responses of human subjects to several vaccines is well established.[17–20] Age, sex, genetics, and a complex interplay between the microbiome, cell metabolism products, immune subset frequency, and circulating levels of chemokines and cytokines at both pre-vaccination and early post-vaccination time points all contribute to this heterogeneity.[18,21–23] Unbiased and computational analyses of large "OMICs" datasets, including transcriptomics, proteomics, and metabolomics, have enabled the assessment of the contributions of these factors and the identification of correlates of immunogenicity and protection. Transcriptional profiles early post-immunization that predicted the Ab response to the live attenuated yellow fever vaccine YF-17D,[24,25] influenza vaccine,[26] hepatitis B (HepB) vaccine,[17] and HIV vaccine[27] were identified using such approaches.[28,29] These studies showed the coordinated induction of a strong pro-inflammatory response that included genes of the interferon (IFN) and IL-1 signaling pathways. An early post-vaccination transcriptome signature for DENV was identified following TAK-003 vaccination, including a positive contribution of IFN pathways, B cell cycle, and dendritic cell (DC) antigen-presentation modules.[30] Moreover, pre-vaccination transcriptional signatures for influenza, HepB, malaria, and yellow fever vaccination[17,19,31,32] also have been identified. These profiles have shown a consistent association of pre-vaccination inflammation (IFNs and NF-κB) with variation in vaccine response. Nonetheless, the mechanisms and upstream regulators of these pre-vaccination signatures remain undefined.

Given the increased rate of infection observed in seronegative individuals immunized with Dengvaxia, we leveraged multi-OMICs data from a phase II clinical trial (ClinicalTrials.gov, NCT01696422) testing the immunogenicity of the live attenuated tetravalent Butantan-DV/TV003 vaccine in Brazil[33–35] to identify correlates and mechanisms that promote a broad nAb response, the surrogate marker of vaccine-mediated protection. Integration of transcriptomics, metabolomics, proteomics, flow cytometry, and validation in human primary monocytes identified the balance between pro- and anti-inflammatory transcriptional and metabolic signatures in monocytes as a correlate and a mechanism upstream of a broad nAb response in seronegative participants.

RESULTS

Breadth of DENV-specific Ab responses is a feature of vaccine responses triggered by the Butantan-DV/TV003 vaccine

We used samples from the phase II clinical trial, registered at ClinicalTrials.gov (NCT01696422) (Figure 1A), to define correlates of broad nAb responses to all four DENV serotypes. A total of 35 seronegative individuals were immunized, with a second dose administered 180 days after the first dose. Participant demographics are outlined in Table 1. The Butantan-DV/TV003 vaccine induced a potent multivalent nAb response (>2 serotypes) in most individuals ($n = 30$) as determined by plaque reduction neutralization tests (PRNTs), and this response was detectable in the plasma of vaccine recipients for at least 90 days after immunization (Figure S1A; Table S1). The Ab response was induced principally after primary immunization, as boosting did not increase nAb titers nor the breadth of the Ab response to all four serotypes. The kinetics and magnitude of the primary response varied across serotypes and participants (Table S1). The capacity to neutralize (titer >10) DENV1, DENV2, and DENV4 serotypes was detected in 84.9%–87.9% of participants at day 91 and 53.6%–85.8% of participants at day 180. Of note, the nAb response to DENV3 was less durable than that to the other three serotypes, with an average of 111 days of seropositive nAb response (versus 153, 133, and 149 for DENV1, DENV2, and DENV4, respectively), with significant differences compared to the DENV1 and DENV4 responses (Tables S2 and S3). We identified three non-responders (8.5%); the plasma of these subjects could not neutralize any of the four serotypes in PRNTs at any time point before day 90. The peak response, defined as the time point showing the highest Ab titers against DENV1 and DENV3 (48.4% and 54.8%, respectively), occurred at day 28 for close to half of the participants, whereas for others it occurred between days 56 and 91 (Table S4). In contrast, peak neutralizing titers for DENV2 and DENV4 were delayed, with the highest titers observed

(B) UpSet plot of differentially expressed genes (DEGs; $p < 0.05$) at the pre-vaccination time point associated with post-vaccination outcomes. Each row represents an outcome, with the number of DEGs at the far right. Genes positively and negatively associated with each outcome are indicated in red and blue, respectively. Bar plots above indicate the number of DEGs in common across selected outcomes. Degrees indicate the number of outcomes included in each intersection.

(C and D) Heatmaps representing pathway EnrichmentMap analysis for immune (C) and metabolic (D) transcriptomic gene sets, where each row represents a pathway module and columns represent individual participants. Column annotation tracks (top) represent the breadth per participant. The dataset contains 8 and 24 biological replicates for low and high breadth, respectively.

(E) Cartoon depicting the association of breadth correlates for low (left) and high (right) breadth.

Table 1. Demographics of phase II Butantan-DV/TV003 vaccine-seronegative participants

	DENV-naive participant groups	
	Placebo (n = 11)	Vaccine (n = 35)
Sex		
Women	8 (73%)	24 (69%)
Men	3 (27%)	11 (31%)
Age (years)	37.8 (9.58)	41.6 (11.78)
Weight (kg)	76.1 (25)	73.7 (22)
Height (m)	1.6 (0.05)	1.7 (0.13)
Race/ethnicity		
White	5 (45%)	21 (60%)
Black	1 (9%)	2 (6%)
Pardo	3 (27%)	8 (23%)
Asian	1 (9%)	1 (3%)
Other	1 (9%)	3 (9%)
YF-17D vaccination status		
Unvaccinated	6 (55%)	14 (40%)
Vaccinated	4 (36%)	13 (37%)
Unknown	1 (9%)	8 (23%)

Data represent mean (SD) for age, weight, and height, and n (%) for the rest of demographic variables. nAb responses to the DENV serotypes were validated in each group, and results show with PRNT values ranging between 10 and 5,120.

at day 56 (45.2% and 48.4%, respectively). The kinetics of the neutralizing response to each serotype was variable, as for most vaccinees individual serotype responses did not peak at the same time point (Tables S4 and S5).

The heterogeneity in the kinetics of the serotype-specific nAb titers prompted us to use the $\log_{10}$-transformed area under the curve (AUC) values to assess the magnitude of the Ab response per participant between days 0 and 90. Breadth was defined as a detectable nAb response (titer >10) to all four DENV serotypes irrespective of the time point post-immunization. These criteria identified two groups of vaccine recipients where high breadth, a prerequisite of a protective immune response to the vaccine in seronegative vaccinees, was defined by a detectable nAb response to all four serotypes and low breadth (i.e., non-protective response) by DENV-specific Ab responses to three or fewer serotypes.[11,36] We detected no significant association between clinical features (Table 1) such as age, sex, body-mass index (BMI), and race or prior YFV-17D vaccination status and breadth. Figure S1B shows the distribution of participants in regard to their response to individual serotypes: rows represent conditions for which the number of participants are met (bar plot; top), colored by number of degrees of intersections. Most participants (26 of 35, 74.3%) mounted the protective high-breadth (four degrees across all serotypes, in red) response at day 90 (Figure S1B), with the remaining (9 of 35, 25.7%) defined as low-breadth participants. The latter all mounted a detectable nAb response against DENV1 (with the exception of the aforementioned non-responders to all four serotypes), suggesting that this serotype was the most immunogenic for inducing nAb responses. In contrast, DENV3 responses were lacking in low-breadth individuals, where seven of nine participants (including the three non-responders to all four serotypes) did not achieve detectable DENV3-specific nAb titers. These results suggest that the DENV3 serotype is a driver of breadth response following immunization.

Type I IFN and TGF-β signaling dichotomy as drivers of breadth of the nAb response to Butantan-DV/TV003

Transcriptomic profiling of peripheral blood mononuclear cells (PBMCs) collected pre-vaccination from all donors identified genes associated with an optimal response to the vaccine (Figure 1A). Unsupervised principal-variance-component analysis (PVCA) revealed a weak association (0.43%) with breadth. Biological sex and race were the largest drivers of the pre-vaccination variance across samples with respectively 22.04% and 11.85%. These features did not contribute to the differences observed in breadth (0.3% and 0%, respectively) (Figure S2A). Unsupervised principal-component analysis (PCA) confirmed these findings (Figure S2B). A supervised analysis (DESeq2) enabled us to identify 530 and 609 genes, respectively, that were associated before vaccination with the high and low breadth of the nAb response (nominal $p < 0.05$) (Figure S2C).

The number of differentially expressed genes (DEGs) associated with nAb AUC varied across serotypes (Figure 1B, right margin), with 1,471 DEGs (661 up, 810 down) for DENV1, 1,434 DEGs (816 up, 618 down) for DENV2, 2,427 DEGs (1,265 up, 1,162 down) for DENV3, and 1,155 DEGs (527 up, 628 down) for DENV4. DEG similarity across breadth and serotype-specific AUC outcomes was characterized using number of intersecting DEGs (Figure 1B, top) between 2 and 4 outcomes, where colors represent the number of outcomes intersected. This analysis showed that DENV3 had the highest overlap with high-breadth DEGs (n = 465); in contrast, DENV1 showed low overlap with high-breadth DEGs (n = 94) (Figure 1B). This reflects our observations about the large differences in magnitude of the nAb response to DENV3 between high- and low-breadth participants and suggests that factors that determine breadth are also involved, at least in part, in regulating the DENV3 nAb response.

Pre-ranked gene set enrichment analysis (GSEA) revealed significant associations of the breadth of Ab responses to DENV serotypes with several biological pathways as quantified by normalized enrichment score (NES). We identified a total of 3,489 gene sets associated at a nominal $p < 0.05$ (2,849 associated with high breadth and 625 with low breadth) or 1,039 at an adjusted p (false discovery rate [FDR]) < 0.05 (799 high; 240 low). EnrichmentMap was used to generate modules based on similarity (Jaccard similarity index cutoff of 0.25) between significant gene sets ($p < 0.05$). We identified 27 gene modules that highlighted specific immune effector functions (Figure 1C), 10 of which were associated with high breadth, whereas 17 were associated with low breadth. This analysis revealed a positive association (p values ranging from 0.008 to 0.0002) of transcription factor (TF) downstream signatures, including SMAD2/3/4 and ETS-1; these TFs control the expression of *CXCR4*, *CCR4*, *IL7R*, *IL6R*, and *RUNX1* genes and are associated with high breadth of DENV-specific responses. In contrast, expression of pro-inflammatory genes, including *TNFA* and *RELA* (p < 0.01–0.00183), was negatively associated with breadth of DENV-specific neutralization. The strongest association with low breadth included two

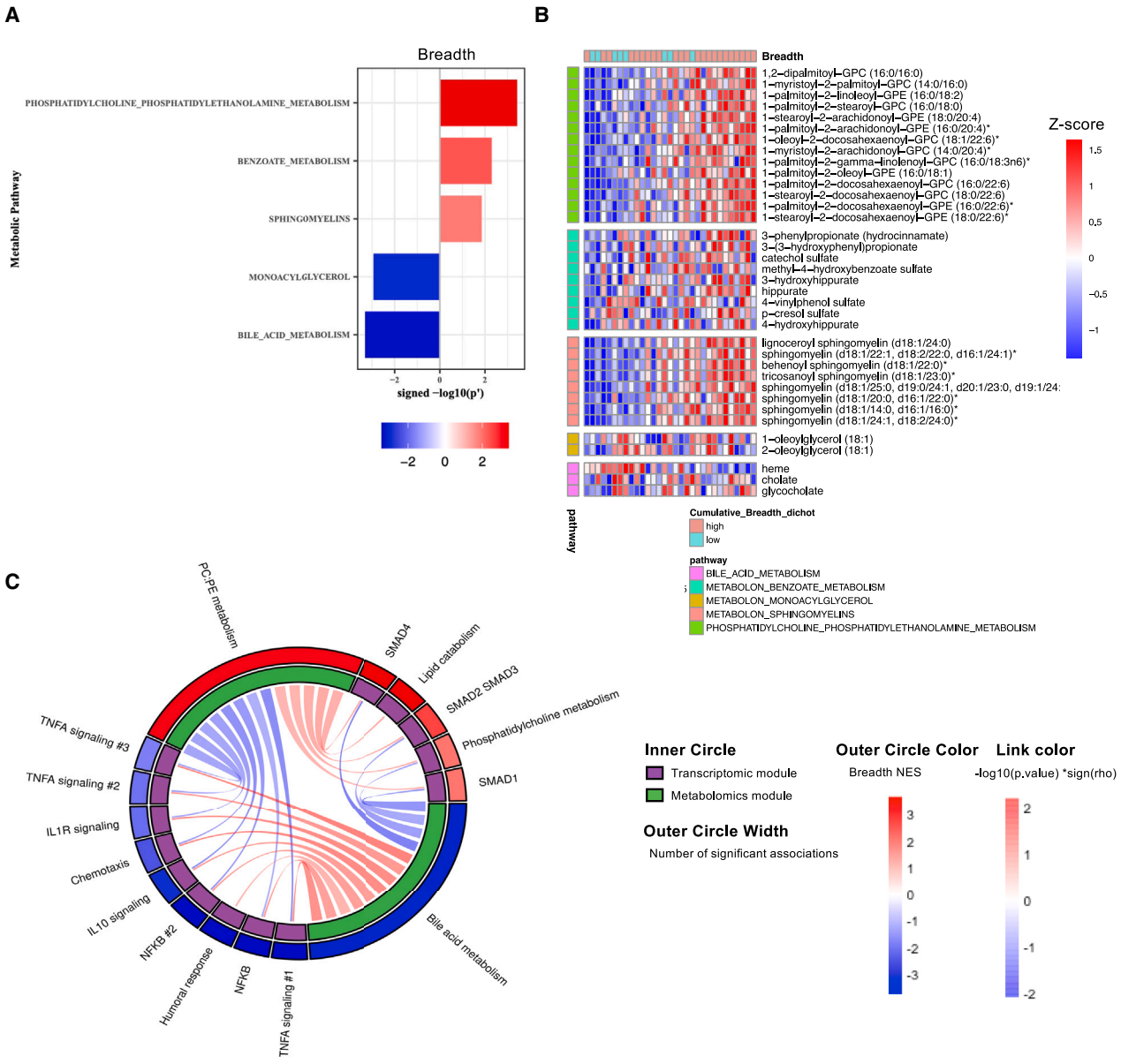

(legend on next page)

modules of genes regulated by type I IFNs (<0.00018), including those with established antiviral functions (*IFIH1*, *DDX58*, *IRF1*, *IFIT1*, *IFIT2*, and *IRF7*) and tonic IFN signaling (*STAT1*, *USP18*, and *PARP9*) (Figure S3A).[37–40] IFN gene signatures, especially those with ascribed antiviral functions and including *DDX58*, which encodes the cytoplasmic viral RNA (including for Flaviviruses) sensor RIG-I,[41–43] were negatively associated with the DENV3-specific nAb response; in contrast, DENV1-specific responses were not impacted by the expression of these genes (Figure S3B). DENV2-specific responses were also associated with the expression of these interferon-stimulated genes (ISGs) in terms of number of significant genes, albeit to a lesser degree of significance than DENV3. Thus, variations in sensing of viral RNAs across participants could affect the breadth of the nAb response. Genes encoding pro-inflammatory cytokines identified in the pathway analysis (Figure S2D) were negatively associated with breadth at a univariate level; they included *IFNG* and members of the IL-1 family (*IL1B* and *IL1A*) or cytokines induced by IL-1 signaling (*IL6*). We also identified several chemokines enriched in the low-breadth group (e.g., *CCL3*, *CCL4*, *CXCL1*, and *CXCL3*) and one in the high-breadth group (*CCL2*), which is consistent with the chemotaxis module being negatively associated with breadth (Figure 1C).

We used the TGFB signaling and type I IFN signatures, including subsignatures of the tonic and antiviral IFNs,[39] to validate our findings in other live attenuated pre-vaccination datasets from the Human Immunology Project Consortium (HIPC).[44] We performed differential expression analysis between high and low responders for the magnitude of the Ab response in parallel for each trial and leveraged the results for GSEA using our signatures (Figure S3C). Enrichment of type I IFNs, along with antiviral ISGs and tonic IFN signaling, was associated significantly in low responders from two of three vaccine trials with another live attenuated flavivirus vaccine, YFV-17D. The third YFV study (SDY1264) exhibited an enrichment for IFNs in the high responders, which reflected the pre-vaccination profile observed for another live attenuated vaccine, namely varicella zoster.[45] Of note SMAD2/3/4 modules (Figure S3C) were enriched in three of four YFV-17D vaccine trials, corroborating our observations in the Butantan-DV/TV003 DENV vaccine trial.

Pre-vaccination metabolic activity as a driver of the breadth of DENV-specific Ab responses to Butantan-DV/TV003

Intracellular metabolic pathways (i.e., oxidative phosphorylation, fatty acid oxidation, and glycolysis) and metabolites derived from the microbiome that translocate to systemic circulation (bile acids [BAs] and short-chain fatty acids) have been shown to regulate innate and adaptive immune responses following vaccination.[46,47] Given these data, we investigated whether pre-vaccination transcriptomic signatures of cell metabolism also could predict breadth of vaccine responses (Figure 1D). We identified several metabolic pathways that were positively associated with high breadth, including pathways of mitochondrial function (NAD metabolism, oxidative stress, glycolysis, amino acid metabolism, and lipid metabolism; p values ranging from 0.0006 to 0.00033).

Systemic metabolites have been shown to trigger differentiation of effector cells of the innate and adaptive immune responses.[46,48,49] We analyzed a broad panel of 868 pre-vaccination plasma metabolites and correlated these data with breadth of the nAb response (Figure S4A). We identified 22 differentially expressed metabolites (nominal p <0.05) across breadth groups including many different classes of metabolites, six of which belonged to the phosphatidylcholine (PC)/phosphatidylethanolamine (PE) class.

We performed pathway analysis using metabolite set enrichment analysis (MSEA) on the Small Molecular Pathway DataBase (SMPDB) and Metabolon metabolite sets followed by EnrichmentMap to identify consolidated metabolic modules from overlapping metabolite sets with high degrees of redundancy in metabolite composition (Jaccard distance <0.5). Figures 2A and 2B show the statistically significant metabolic modules and their associated overrepresented core metabolites (i.e., enriched in multiple pathways in a given module). PC/PE metabolism positively correlated with the breadth of nAb response (p = 0.00037) (Figures 2A and 2B), confirming our observations from the univariate analysis (Figure S4A). We highlighted the strongest drivers of module enrichment from the core metabolites of correlates in Figure 2A; PC/PE metabolism includes 14 metabolites. Other modules that correlated positively with the breadth of the vaccine response included benzoate and sphingomyelin metabolism (p = 0.005 and p = 0.013). Sphingomyelins are a degradation by-product of PCs[50] and trigger TGF-β activation in regulatory T cells (Tregs), which impacts their function. In contrast, we observed a significant association of the primary BA cholate (CA) and glycocholate (GCA) as negative correlates of the breadth of the Ab response (p = 0.00049). The identification of these metabolites confirms the importance of systemic/circulating metabolites, which were also confirmed by the enrichment of metabolic pathways in pre-vaccination transcriptional profiles (Figure 1D).

Figure 2. Pre-vaccination profiling of plasma metabolites reveals that metabolic pathway activity is associated with inflammatory status

(A) Metabolite set enrichment analysis (MSEA) was performed on pre-ranked metabolites from differential expression analysis, followed by EnrichmentMap analysis with a Jaccard index >0.5 for modules displaying a nominal $p < 0.05$. Bar plot represents individual modules, with the signed $-\log_{10}(p$ value) as a metric for the association with breadth, where red and blue respectively denote an association with high and low breadth.

(B) Heatmap representing the core metabolites from modules in (A), where each row represents normalized metabolite expression and columns represent individual participants. Row annotation tracks (left) represent the signed log p value of the association of each outcome for each module, with blue and red denoting high negative and positive significance, respectively. Column annotation tracks (top) represent the outcome per subject. The dataset contains 8 and 23 biological replicates for low and high breadth, respectively.

(C) Integrated correlation network analysis of transcriptomics and metabolomics, where nodes denote features and edges the correlation coefficient between the two features they link. Spearman correlation ($p < 0.05$) was used as an integration metric across OMICs and displayed on the edge color. Node shape and color map to the respective feature type and association with neutralization breadth.

(D) Cartoon depicting the association of breadth correlates for low (left) and high (right) breadth.

A correlation analysis between transcriptomic and metabolic sets confirmed the association between metabolic pathways across RNA sequencing (RNA-seq) and metabolomics data for the leading positive and negative metabolic pathways that could drive inflammation (Figure 2). This analysis highlighted the interplay between specific metabolic pathways and inflammatory activity, where BA metabolism modules were positively correlated to nine pro-inflammatory transcriptional profiling modules, including type I IFN, TNF-α signaling, IL-1R signaling, and NF-κB signaling, and PC/PE metabolism was negatively associated with these pro-inflammatory pathways. Instead, PC/PE was correlated to five positive transcriptomic determinants of breadth of neutralization, three of which are involved in TGF-β signaling (SMAD1, SMAD2/3, and SMAD4). Given that PC/PE and BA pathways displayed the strongest association with breadth and transcriptomic inflammatory pathways (at the pathway and analyte levels), they were prioritized for further analyses. These observations also highlight the extent of immunological and metabolic pathway crosstalk associated with an optimal response to Butantan-DV/TV003. Given the strong association with multiple cytokine signaling pathways and chemotaxis, we searched for cytokine/chemokine genes that correlated to metabolokine levels (Figure S4B) and identified inflammasome-driven cytokines *IL1B*, *IL18*, and *IL-6* as associated with BA levels. In contrast, PC/PE metabolites displayed a negative association with most genes associated with low breadth, including chemokines *CCL4*, *CXCL3*, and *CLXCL1* and the cytokine *IFNG*.[51]

The heterogeneity of pre-vaccination monocytes is associated with the breadth of the nAb response to TV003

We monitored the association of innate and adaptive cell subsets with the breadth of DENV-specific nAb responses using flow cytometry. Unsupervised clustering using a combination of PhenoGraph clustering with the t-SNE dimension reduction approach revealed 22 distinct clusters of innate immune cells among $CD3^-CD19^-CD56^-$(Lin^-) cell subsets (Figure 3A). The frequencies of three of these clusters were significantly associated with the breadth of the nAb response: one cluster of cells expressed a plasmacytoid dendritic cell (pDC) phenotype ($Lin^-CD11c^-CD123^+$; cluster 8, $p = 0.0062$), whereas the two others included monocytes ($CD14^+CD16^-CD11b^+HLA\text{-}DR^+$; clusters 1 and 16) (Figures 3B and S5C). These two monocyte clusters were distinguished by their expression levels of the scavenger receptor CD68. $CD68^{high}$ monocytes (cluster 1) were enriched in the low-breadth group ($p = 0.0028$), whereas $CD68^{low}$ monocytes (cluster 16) were enriched in the high-breadth group ($p = 0.0024$) (Figure 3C). Flow cytometric characterization of the B cell compartment highlighted additional differences between high- and low-breadth responders. The B cell panel, pre-gated on live $CD19^+$ cells, resulted in the identification of 27 clusters (Figures S5B and S5D), two of which were enriched in the high-breadth group. Cluster 8 had a naive B cell phenotype ($CD20^+CD21^+BCL2^{high}IgG$) ($p = 0.03$), whereas cluster 15 had a germinal center (GC) B cell phenotype ($CD20^{high}CD21^{low}CD38^{int}IgD^{low}$) ($p = 0.008$) (Figures 3D and S5B).

We thus hypothesized that monocytes were the key drivers of the crosstalk between immunological and metabolic pathways highlighted in Figure 3C. For this to be true, monocytes would need to meet two prerequisites: they first would need to have higher expression of key transcriptional signatures identified in bulk transcriptomics that correlate to metabolite expression (Figure 2C) relative to other subsets, such as type I IFN and TGFB1 signaling. Second, they would need to express receptors/transporters necessary for signaling of BAs and PC/PE metabolites. To test this hypothesis, we leveraged CITE-seq data generated in an influenza pre-vaccination study ($n = 20$ subjects; Figure 4).[19] We first verified the expression of these genes across different cell identities. Cell identities were inferred from reference-based annotation (SingleR with a Monaco reference[52,53]) and then validated with surface marker expression (Figures 4A and S6). We then validated that myeloid cells, particularly monocytes, exhibited higher expression of *CD68* (Figure 4B). Furthermore, myeloid cells displayed higher expression of *TGR5* (Takeda G-protein-coupled receptor 5 protein, encoded by *GPBAR1*) and the vitamin D receptor *VDR* and nuclear receptor 4A1 (*NR4A1*), both of which serve as BA receptors.[54,55]

PE/PC can putatively signal through CD300A[56] and TIM-1 (*HAVCR1*)[57]; alternatively, STARD7[58,59] and STARD10 transporters[60] can trigger the internalization of these metabolites to the mitochondria. *CD300A* was expressed at highest levels in natural killer (NK) cells, followed by myeloid cell phagocytes, whereas TIM receptor was expressed primarily in T cells. STARD7 was also enriched in myeloid phagocytes, along with B cells, whereas *STARD10* was expressed at lower levels across most immune subsets, including monocytes (Figure 4B). Altogether, these results highlight that innate immune cells, especially monocytes and DCs, likely can respond to both BAs and PC/PE.

We then compared averaged gene expression for genes found in transcriptional modules in Figure 1C across cell identities of the single-cell RNA-seq data and then generated module scores with the GSVA *Z*score method (Figure 4C). A majority of modules were enriched in myeloid cells, but some key modules were found enriched in other subsets, such as humoral response in B cells. More importantly, TGF-β signaling modules such as SMAD2/3 and SMAD4, which were a correlate of high breadth in our data, were enriched in both monocytes and DCs. Moreover, the type I IFN module, which was a correlate of low breadth, was enriched only in monocytes and not in DCs. Among those ISGs, we observed an enrichment of antiviral genes in monocytes, such as OAS2/3, OASL, IFIT3, and TRIM25. We also added BA metabolism gene sets in this analysis, divided into three categories: biosynthesis, transport, and signaling. Similar to other modules, myeloid cells expressed higher levels of genes associated with these functions, further reinforcing the idea that they are at the center of an immunometabolic nexus downstream of BA and PC/PE.

Integrative analysis of Butantan-DV/TV003 OMICs reveals monocytes as central mediators of an inflammation-metabolism crosstalk

We used sparse least-squares regression models[61] to investigate whether the gene expression signatures associated with breadth of the nAb response in the Butantan-DV/TV003 phase II trial correlated with significant features from plasma proteins, plasma metabolites, and flow cytometry (FCM) subset frequencies datasets

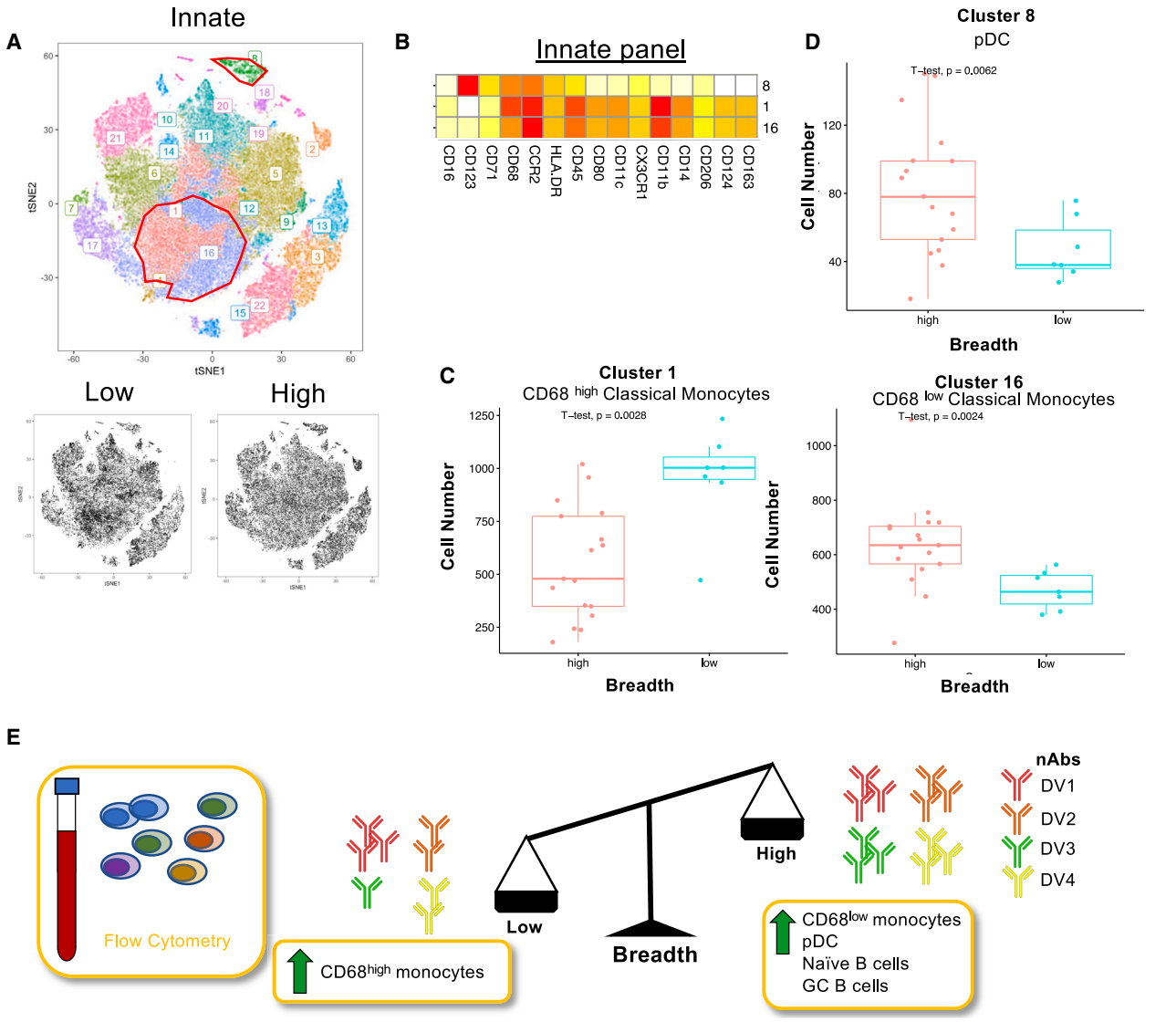

Figure 3. The frequency of pre-vaccination monocyte subsets distinguished by their expression of the scavenger receptor CD68 at the pre-vaccination time point is associated with breadth of the response to Butantan-DV/TV003 in a dichotomous fashion

(A) t-SNE plot of $CD3^{-}CD19^{-}CD56^{-}$ PBMCs from unsupervised flow cytometry analysis. Different colors represent distinct clusters following Rphenograph clustering analysis (top). The t-SNE plot was separated on the basis of breadth outcome (bottom), showing variations in density in clusters 1, 16, and 8. The dataset contains 8 and 17 biological replicates for low and high breadth, respectively.

(B) Heatmap showing scaled median fluorescence cluster profile for each marker: each row is a significant cluster and each column is a marker in the panel. White denotes low expression, while red denotes high expression.

(C) Boxplots showing monocyte clusters 1 (left) and 16 (right) cell frequency versus breadth.

(D) Boxplot showing pDC cluster 8 cell frequency versus breadth.

(E) Cartoon depicting the association of breadth correlates for low (left) and high (right) breadth.

from Figures 1, 2, 3, and 4 (Figure 5). This integrative analysis showed a distinction between pro- and anti-inflammatory pathways and their respective association with $CD68^{high}$ and $CD68^{low}$ monocytes. $CD68^{low}$ monocytes had an enhanced anti-inflammatory TGF-β signaling bias, whereas $CD68^{high}$ monocytes were associated with a pro-inflammatory phenotype. pDC frequencies also were positively associated with SMAD4 and not correlated to pro-inflammatory signaling. Furthermore, as shown in Figure 2C, PC/PE metabolites correlated positively with SMAD4 signaling and negatively with pro-inflammatory modules, including type I IFN, IL-1R, and TNFA signaling. Conversely, BAs showed a positive association with pro-inflammatory modules and a negative association with a SMAD4 response. Altogether, this integrative analysis provides mechanistic explanations for vaccine immunogenicity, whereby metabolites, including BAs and PC/PE, could serve as upstream regulators

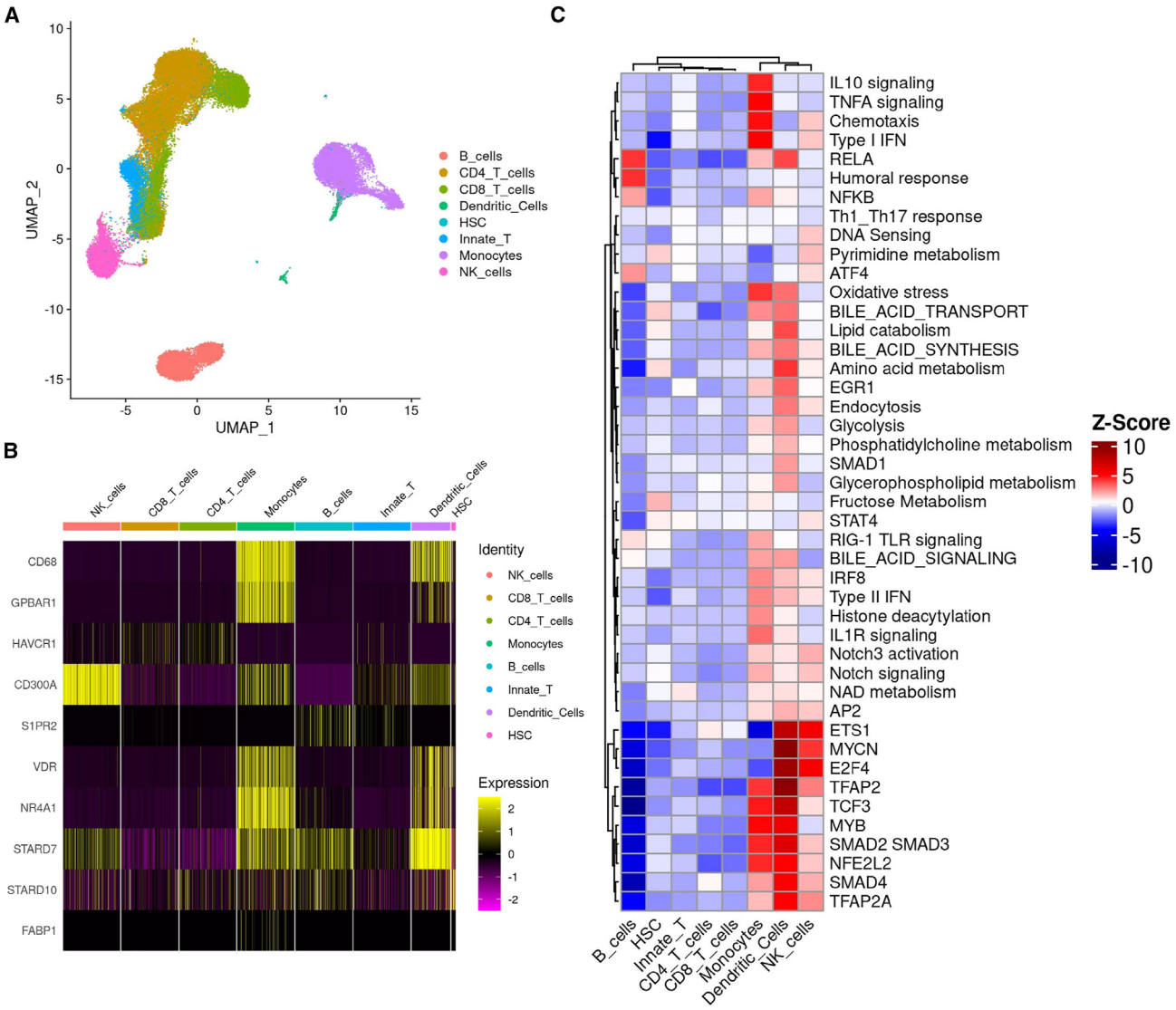

Figure 4. Single-cell transcriptomics analysis on influenza pre-vaccination dataset highlights monocytes as key drivers of immune metabolic crosstalk

(A) UMAP plot of influenza pre-vaccination PBMC CITE-seq from 20 healthy donors. Colors represent cell identity.

(B) Heatmap of single-cell gene expression values for CD68, bile acid receptors, and PC/PE transporters. Yellow and purple denote a higher or lower expression per gene, respectively.

(C) Pathway activity from each dengue transcriptional module per cell identity from averaged gene expression. Each row represents normalized expression per module, while columns represent cell identities. Red denotes higher relative expression, while blue represents lower expression.

to differentially polarize monocyte functions by modulating cytokines such as TGF-β, IL-1β, TNF-α, and type I IFNs.

Metabolite stimulation *ex vivo* shows the contrasting immunomodulatory functions of BA and PC/PE on primary human monocytes

To confirm the immunomodulatory function of these metabolites, we isolated and purified $CD14^{+}CD16^{-}$ monocytes using negative selection and magnetic beads from fresh healthy donor PBMCs (n = 3–6; varies across experiments). Given the association of BA with pro-inflammatory pathways, we exposed monocytes to primary (GCA) or secondary (lithocholate [LCA]) BAs for 6 to 18 h and measured the production of pro-inflammatory cytokines, including IFN-β, IFN-γ, IL-6, IL-1β, IL-8, and IL-18, in culture supernatants using the Mesoscale Discovery platform. Given the documented association of BAs with inflammasomes combined with the association to IL-1 family cytokine expression, we designed a BA stimulation experiment aimed at quantifying inflammasome activation. Thus, all conditions were first primed with lipopolysaccharide (LPS), including the DMSO vehicle, and then exposed to BA. Nigericin was used as a positive control. Viability assays were performed to establish an

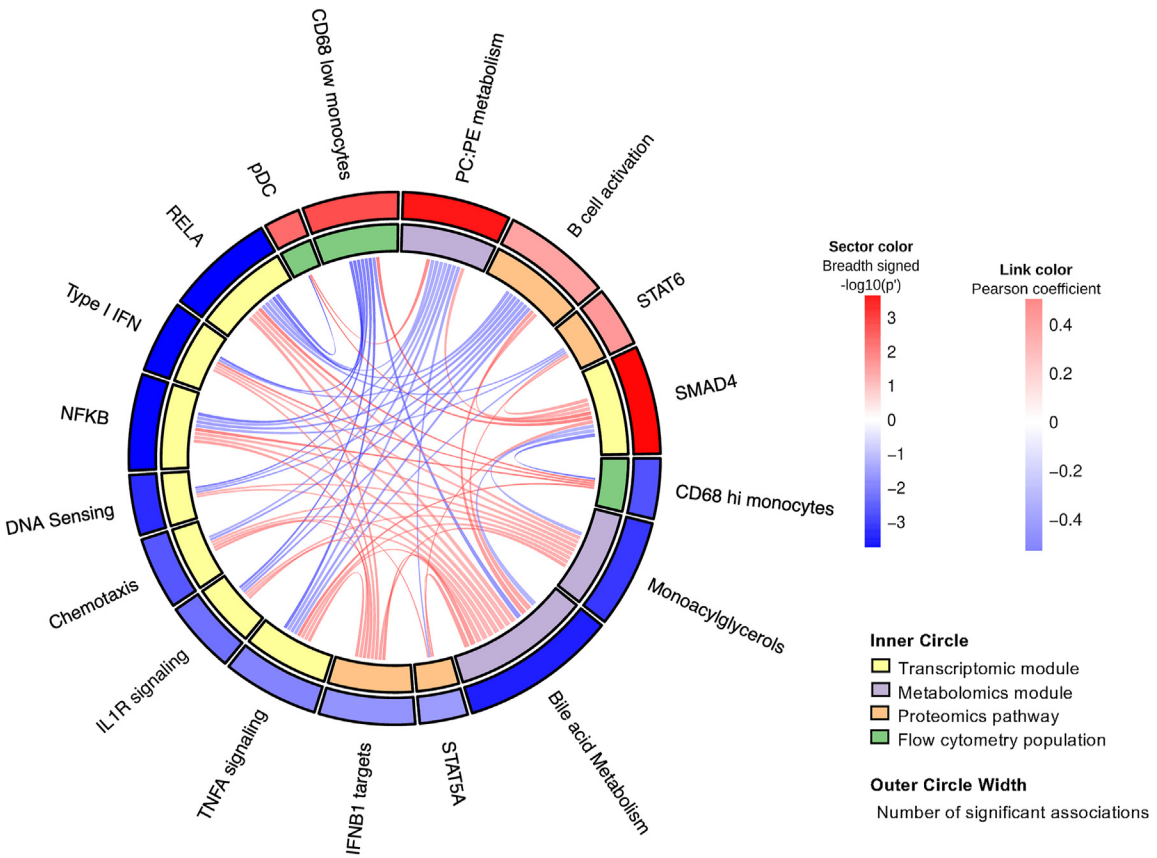

Figure 5. Integrative analysis between transcriptomics, plasma proteomics, and metabolomics and flow cytometry highlights a dichotomous crosstalk of monocyte subsets with metabolic and pro- and anti-inflammatory pathways

Circos plot representation of cross-platform correlation analysis, where nodes denote features and edges the correlation coefficient between the two features they link.

optimal non-toxic dose of BA (Figure S7B). The selected non-toxic concentrations also induced optimal levels of pCREB1 and caspase-1 activation (Figure S7C). We used the time point at which peak responses to each BA were observed among donors. We noted a significant induction (2- to 5.6-fold) of IFN-β (and to a lesser extent IFN-γ by GCA) after exposure to primary or secondary BAs (Figure 6A) compared to the DMSO control. We also observed a significant increase in FLICA^{+} (a fluorescent marker for caspase-1 activation) monocytes 30 min after GCA (p = 0.029) or LCA (p = 0.123) exposure (Figures S7C and S7D). Activation of caspase-1 and production of IL-18, but not IL-1β, were induced by LCA (p = 0.0577), but not by GCA. Together, these data support a pro-inflammatory role for BAs in primary human monocytes.

Monocytes were cultured in serum-free medium and stimulated with PC/PE for 12 and 20 h, followed by measurement of TGF-β1 production. Both PC and PE induced a 100- to 1,000-fold increase in TGF-β1 production compared to controls (Figure 6C). This TGF-β1 increase after PE exposure was associated with a reduction in the expression of the latent activated peptide (LAP) on the surface of CD68^{high} monocytes (p = 0.028; Figure S7E). Higher levels of TGF-β1 triggered SMAD2/3 phosphorylation in CD68^{high} but not in CD68^{low} monocytes (Figure 6B). Given the differences in levels of pSMAD and LAP expression between CD68^{high} and CD68^{low} monocytes, we characterized the baseline phenotype of unstimulated cells (Figure S7F): CD68^{high} monocytes showed higher expression of GARP, a receptor for TGF-β that regulates its activation in Tregs,[62,63] and a marked reduction in expression of LAP compared to CD68^{low} monocytes. This distinction suggests a differential capacity for TGF-β activation at pre-vaccination by the two monocyte subsets. Exposure of monocytes to PC and PE led to a significant downregulation of CD68 as judged by the ratio of CD68^{high}:CD68^{low} cell frequencies (Figure 6D); this shift in ratio upon *ex vivo* exposure to PC/PE correlates with the differences observed in the pre-vaccination cohort between high- and low-breadth responders for clusters 1 and 16 (Figure 3C).

Finally, we developed an *ex vivo* model to confirm that TGF-β production triggered by PC/PE would counterbalance the pro-inflammatory IFN response induced by viral pathogen-associated molecular patterns (PAMPs) present in the live attenuated Butantan-DV/TV003 vaccine.[64] We conditioned primary monocytes with PC/PE (12 and 20 h), followed by treatment with the TLR7/8 agonist R848 for 24 h as a surrogate for DENV infection (Figure 6E).[65] Four cytokines and chemokines (CX3CL1, IFN-α2α, IL-10, and IL-1β) induced by R848 and repressed by

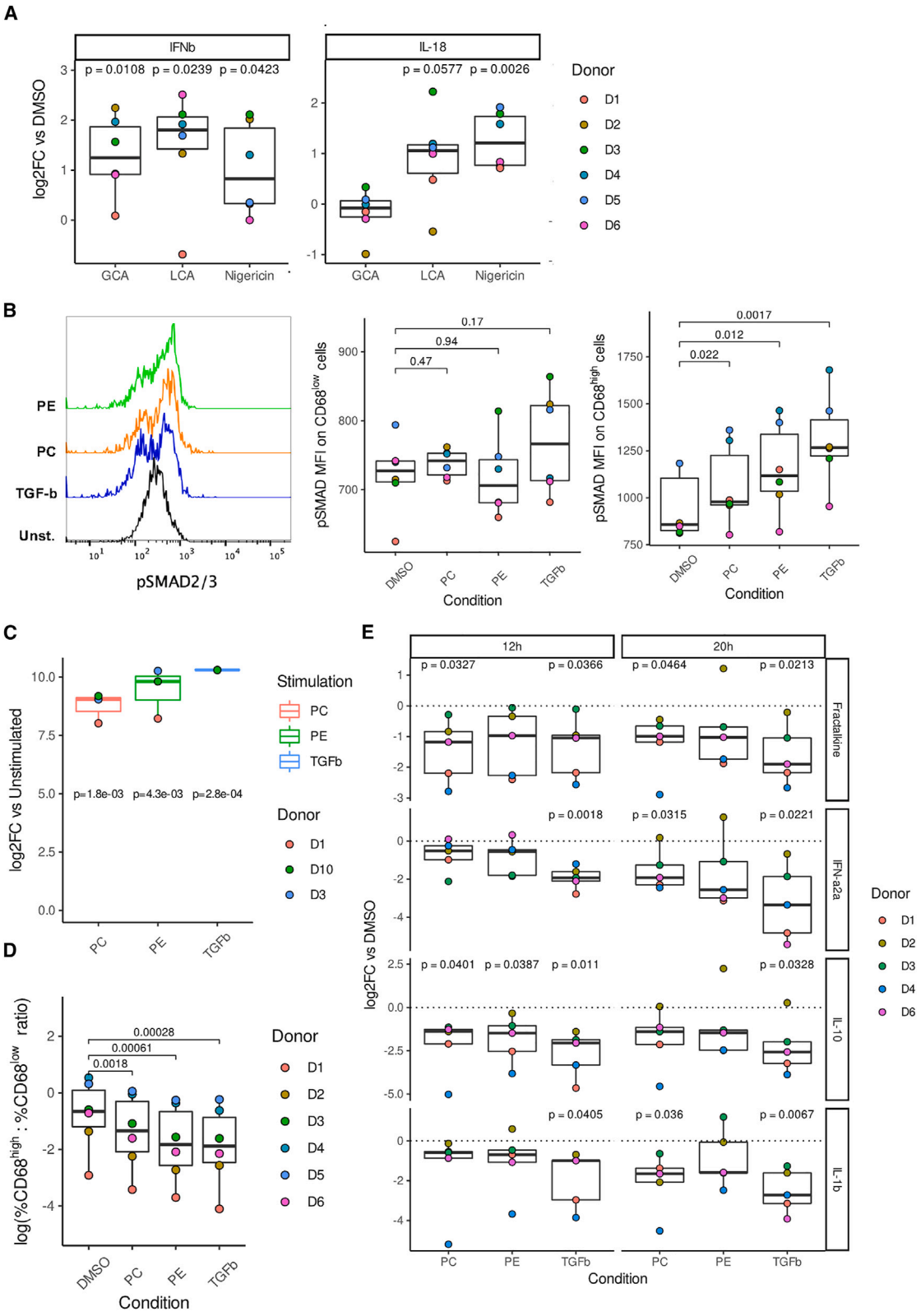

(legend on next page)

exogenous TGF-β were also repressed by PC, PE, or both PC and PE treatment at 12 and/or 20 h ($p < 0.05$). CX3CL1 expression was preferentially inhibited by PC at both time points. Moreover, IFN-α2α and IL-1β, both triggered by BAs, were inhibited by PC at the 20 h time point. Of note, PC and PE treatment dampens IL-10 production, which is known to promote GC reactions.[66,67] Taken together, the results of our integrative analysis and experimental validation highlight the crosstalk and interplay between pro- and anti-inflammatory signatures driven by metabolic reprogramming and their impacts on the breadth of Ab responses in the context of immunization with a replicating viral vaccine.

DISCUSSION

In this study, we leveraged an in-depth multi-OMICs analysis of DENV vaccination to provide a mechanistic framework that underlies the impact of the cell-intrinsic and systemic metabolome on immunogenicity in subjects prior to immunization with a live attenuated DENV vaccine. This phase II trial included 35 seronegative participants. These individuals were vaccinated with the Butantan-DV/TV003 vaccine in Brazil. We showed that the response to this tetravalent vaccine was heterogeneous at multiple levels, including the breadth, the magnitude, and the kinetics of the response. This heterogeneity prompted an investigation into host signatures prior to vaccination that could have an impact on the breadth of the nAb response to the four DENV serotypes present in the vaccine; the emphasis on the breadth of the response is critical in preventing ADE.[33] We identified a network of BA and PC/PE metabolites that respectively trigger the activation of pro- and anti-inflammatory signaling cascades in monocytes and modulate the breadth of the humoral immune response to DENV. These findings were validated by stimulating primary monocytes with metabolites that were associated with the breadth of the response to the Butantan-DV/TV003 vaccine.

Associations of the anti-inflammatory properties of PC/PE have been reported, as they trigger the downregulation of TNF-α signaling[68] and autophagy, although the association of PC/PE is unheard of in the context of vaccination. PE deficiencies have been associated with the unfolded protein response (UPR)[69] and endoplasmic reticulum stress.[70,71] The mechanisms through which PC/PE induce anti-inflammatory effects are poorly defined. Experiments with rat chondrocytes have shown that PC/PE can activate TGF-β1.[72] Our experiments validated these findings in primary human monocytes, as we observed an increase in TGF-β1 concentrations in supernatants following exogeneous PC/PE exposure and in SMAD2/3 phosphorylation downstream of TGF-β receptor signaling. Furthermore, we confirmed that innate immune signaling downstream of TLR7/8 in primary human monocytes, including the production of antiviral type I and pro-inflammatory type II IFNs, was inhibited by TGF-β production induced by PC/PE. This observation may be explained by SMAD4 dimerization with the SMAD2/3 complex to inhibit transcription of AP1 and IRF-7, thereby reducing innate sensing of viral RNA.[73] Another mechanism of action of PC/PE on TGF-β could be mediated by the binding of phospholipids to CD300A or STARD7, which are found in monocytes and other myeloid cells.[56]

In contrast, exogenous BA stimulation of human primary monocytes induced the production of pro-inflammatory cytokines, including IFN-β and IL-18, which were associated with low breadth. This observation is supported by a recent study showing that children with elevated BA demonstrated poor responses to HepB vaccination.[74] In comparison, modulation of secondary BAs as a result of gut microbiome perturbations altered immunity to influenza vaccination with reductions in influenza-specific IgG1 and IgA production that was partially mediated by effects on inflammasome signaling.[46] This finding contrasts with our data and could be explained by the distinct nature of the vaccine (inactivated versus live attenuated). Our results suggest that BA-induced IFNs impede the response to Butantan-DV/TV003 by limiting viral sensing by innate immune cells. BAs have been known to play an antiviral role in other contexts: administration of deoxycholic acid (DCA) induces antiviral ISG expression in monocytes in the context of CHIKV infection.[75] This BA-induced antiviral effect has been associated with a TGR5-SRC signaling axis.[76] Multiple immune subsets can potentially respond to metabolites such as BA: receptors and transporters necessary for downstream signaling are expressed by monocytes, DCs, NK cells, or B cells. However, only monocytes showed detectable levels of liver fatty acid binding protein (*FABP1*), which has been hypothesized to promote a cytoprotectant effect against toxic fatty acids such as BAs and monoacylglycerols, which would otherwise promote cytotoxicity.[77–79] This implies that expression of receptors is not sufficient for downstream signaling and that monocytes are a likely subset to mediate a response from BAs.

Several studies have focused on understanding the impact of pro- and anti-inflammatory signatures as respective negative and positive correlates of vaccine immunogenicity. Fourati et al. demonstrated hyporesponsiveness to HepB vaccination

Figure 6. BA or PC/PE metabolite exposure respectively induces a pro- or anti-inflammatory response in primary monocytes

(A) *In vitro* supernatant cytokine secretion in primary healthy monocytes following exposure to BAs glycocholic acid (GCA) and lithocholic acid (LCA), following 4 h of LPS priming (1 μg/mL) on 6 biological replicates. Nigericin was used as a positive control for inflammasome-induced cytokines. The y axis represents $\log_2$ fold change versus vehicle DMSO.

(B) Flow cytometry induction of SMAD2/3 phosphorylation following 20 h of PC or PE exposure in $CD68^+$ primary monocytes from six biological replicates. Exogenous TGF-β1 was used as a positive control.

(C) *In vitro* supernatant TGF-β1 secretion following PC/PE exposure for 12 h in primary monocytes on three biological replicates. The y axis represents log fold change versus unstimulated cells per donor.

(D) Log ratio of $CD68^{high}$ versus $CD68^{low}$ monocyte frequency after PC/PE exposure for 20 h from six biological replicates.

(E) *In vitro* supernatant cytokine quantification of cytokine production in primary monocytes from five biological replicates stimulated with R848 for 24 h, followed by PC/PE exposure for 12 and 20 h. The y axis represents the log fold change versus the DMSO vehicle per donor. Parametric paired t test was used for all analyses.

in the setting of heightened inflammation.[17] Similarly, pre-vaccination profiling for RTS,S/AS01 vaccination has shown a heightened IFN antiviral and inflammatory signature in future malaria cases versus controls, suggesting a negative impact of IFN on the vaccine response.[32] In contrast, others have shown a positive association of pre-vaccination IFN responses with tetravalent influenza vaccination,[19] a study for which CD68 expression was a positive correlate of outcome. Similarly, work by the HIPC has shown a pan-vaccine NF-κB- and IRF-7-driven signature as a positive correlate of the magnitude of the Ab response.[44] Networks of genes regulated by these two TFs highlight a pre-vaccination signature that could predict the magnitude of the response to 13 different vaccine platforms. This pan-vaccine signature highlights the negative impact of IRF-7 and IFN-regulated genes on the response to live attenuated viruses; thus, individuals with higher levels of expression of antiviral genes prior to vaccination may abort more rapidly replication of a live attenuated viral vaccine, effectively reducing antigen load and the generation of a potent humoral response; this also is seen by our observation of enrichment of pre-vaccination IFN in low responders to the YFV-17D vaccine. This hypothesis is supported by recent data with another live attenuated DENV vaccine (TAK-003), where the high responders had detectable viremia, whereas low responders did not. Our results show that pre-vaccination antiviral functions, which are modulated by systemic metabolites, influence viral replication of live attenuated viral vaccines and the subsequent Ab response to these vaccines.

Monocytes have been identified as positive or negative correlates of the vaccine response to HepB, malaria, HIV, and YFV vaccination.[17,24,26,31,32] Monocytes include several functional subsets, with markers such as CD9, Slan, CD36, CCR2, CD93, LAIR2, or VCAN,[80,81] identifying new subsets of these cells. Herein, we identified CD68, a macrophage marker, as associated with this functional heterogeneity.[82] CD68 is involved in the binding of oxLDL, phosphatidylserine, and apoptotic cells,[83] and its expression on monocytes could mediate the response to the Butantan-DV/TV003 vaccine by facilitating the uptake of infected apoptotic cells. Alternatively, it could be a surrogate marker of an IFN signature in monocytes that is associated with vaccine outcome to Butantan-DV/TV003 and influenza vaccines, as highlighted by its association with ISG expression and documented status as a target gene of STAT1/2/3.

pDCs were positively associated with the breadth of the nAb response, although this association was not linked to their capacity to produce IFNs.[84] We did observe a positive association of pDCs with PC/PE and SMAD4 signaling, which raises the possibility that production of type I IFNs by pDCs might be inhibited by TGF-β produced in response to PC/PE. pDCs are known to exert regulatory functions, such as the production of IDO and TGF-β.[85] In parallel, we observed a positive association of naive B cells and GC B cells with the breadth of nAb responses. A larger pool of uncommitted B cells and a niche favorable to GC survival and proliferation might favor induction of a broader nAb response.

We have generated a mechanistic model of the pre-vaccination immune state required for a broad and protective DENV vaccine response that would minimize the potential for ADE. We posit that a balance between pro- and anti-inflammatory responses triggered by metabolites present in the host modulates the capacity of a live attenuated vaccine to replicate in monocytes, a key cell that supports DENV spread and antigen presentation.[86,87] Allowing the attenuated virus to replicate by dampening the initial immune response may be beneficial. This could potentially distinguish pre-vaccination signatures for live attenuated vaccines from other vaccine strategies that do not depend on viral replication. The interplay between PC/PE, BA metabolites, and inflammatory pathways before vaccination paves the way for potential pre-conditioning regimens prior to vaccination to optimize responses. Indeed, BAs are induced by a cholesterol-rich diet,[88] which hypothetically could be avoided to reduce the pre-vaccination IFN response. In parallel, PC is present in meat, egg, dairy, some cruciferous vegetables, and beans, some of which could be included in a pre-vaccination regimen.[89] This concept is supported by evidence of the anti-inflammatory impact of oral PC supplementation in ulcerative colitis.[90] In summary, we believe our study offers mechanistic insights into the response to live attenuated vaccines and provides a case for establishing the role of metabolites in modulating anti- and pro-inflammatory responses.

Limitations of the study

This study was performed on human participants of both sexes and across multiple race/ethnicities. We have investigated the impact of these factors on vaccine outcome, inflammatory responses, and metabolic signatures and found no association. However, it is possible that we do not have the sample size to detect modest effects and thus cannot fully exclude their potential involvement. Furthermore, statistical studies using large OMICs (transcriptomics, metabolomics) in healthy subjects at the pre-vaccination time point, including ours, use nominal *p* values instead of adjusted *p* values, because of the presence of modest univariate effects. We compensate for this issue by leveraging pathway analysis (e.g., GSEA) instead of univariate findings, which are more robust to this issue.

STAR★METHODS

Detailed methods are provided in the online version of this paper and include the following:

- KEY RESOURCES TABLE
- RESOURCE AVAILABILITY
  - Lead contact
  - Materials availability
  - Data and code availability
- EXPERIMENTAL MODEL AND STUDY PARTICIPANT DETAILS
  - Human participants
- METHOD DETAILS
  - Flow cytometry staining
  - Metabolite stimulation
  - Cytokine assessment
- QUANTIFICATION AND STATISTICAL ANALYSIS
  - Outcome definitions
  - Transcriptomic analysis
  - Metabolic profiling
  - Unsupervised flow cytometry analysis
  - Single-cell transcriptomic analysis
  - Integrative analysis

SUPPLEMENTAL INFORMATION

Supplemental information can be found online at https://doi.org/10.1016/j.celrep.2024.114370.

ACKNOWLEDGMENTS

We acknowledge A. Talla and A. Sharma for the generation of the t-SNE and PhenoGraph script for unsupervised flow cytometry analysis; J.A. Tomalka for advice on caspase activation experiments; and the Butantan Institute for the management of the phase II TV003 clinical trials. Characterization of the pre-vaccination signature of TV003 was supported by NIAID grant 5R01AI125202-03.

AUTHOR CONTRIBUTIONS

A.-N.P. performed all bioinformatic analyses and some flow cytometry experiments, prepared all the figures, and redacted the manuscript. G.P.S. performed validation experiments and reviewed the manuscript. A.I. generated flow cytometry data and edited the manuscript. M.W. and E.P. generated the proteomics data and initial analysis. T.D.P. and K.I.C. contributed to the testing and design of validation experiments. A.F.-M. performed a bioinformatics analysis of outcomes. A.R.P. oversaw the DV/Butantan clinical trials. E.G.K. performed neutralization titer assays, assisted in the design of experiments, and edited the manuscript. J.K., M.S.D., and E.K.H. assisted with the design of experiments and edited the manuscript. R.P.S. aided in experimental design and setup, data analysis, and generation of figures and wrote the manuscript.

DECLARATION OF INTERESTS

A.-N.P. is a paid bioinformatics consultant and owner of RPM Bioinfo Solutions. M.S.D. is a consultant or advisor for Inbios, Vir Biotechnology, Ocugen, IntegerBio, GlaxoSmithKline, Allen & Overy LLP, Moderna, and Immunome. The Diamond laboratory has received unrelated funding support in sponsored research agreements from Vir Biotechnology, Emergent BioSolutions, IntegerBio, and Moderna. E.G.K. is the current director of the Butantan Institute, which is the vaccine manufacturer. E.P. is a shareholder of CellCarta Biosciences, Inc. T.D.P. is currently employed by MacroGenics, Inc. (Rockville, MD), and received stock options as a condition of employment. R.P.S. is a member of the scientific advisory board for CellCarta.

Received: July 14, 2023
Revised: February 5, 2024
Accepted: May 31, 2024
Published: June 18, 2024

REFERENCES

1. Bhatt, S., Gething, P.W., Brady, O.J., Messina, J.P., Farlow, A.W., Moyes, C.L., Drake, J.M., Brownstein, J.S., Hoen, A.G., Sankoh, O., et al. (2013). The global distribution and burden of dengue. Nature *496*, 504–507. https://doi.org/10.1038/nature12060.
2. van de Weg, C.A.M., Pannuti, C.S., de Araújo, E.S.A., van den Ham, H.J., Andeweg, A.C., Boas, L.S.V., Felix, A.C., Carvalho, K.I., de Matos, A.M., Levi, J.E., et al. (2013). Microbial translocation is associated with extensive immune activation in dengue virus infected patients with severe disease. PLoS Neglected Trop. Dis. *7*, e2236. https://doi.org/10.1371/journal.pntd.0002236.
3. Martina, B.E.E., Koraka, P., and Osterhaus, A.D.M.E. (2009). Dengue virus pathogenesis: an integrated view. Clin. Microbiol. Rev. *22*, 564–581. https://doi.org/10.1128/CMR.00035-09.
4. Guzman, M.G., Alvarez, M., and Halstead, S.B. (2013). Secondary infection as a risk factor for dengue hemorrhagic fever/dengue shock syndrome: an historical perspective and role of antibody-dependent enhancement of infection. Arch. Virol. *158*, 1445–1459. https://doi.org/10.1007/s00705-013-1645-3.
5. Halstead, S.B. (2003). Neutralization and antibody-dependent enhancement of dengue viruses. Adv. Virus Res. *60*, 421–467. https://doi.org/10.1016/s0065-3527(03)60011-4.
6. Halstead, S.B. (1989). Antibody, macrophages, dengue virus infection, shock, and hemorrhage: a pathogenetic cascade. Rev. Infect. Dis. *11*, S830–S839. https://doi.org/10.1093/clinids/11.supplement_4.s830.
7. Halstead, S.B. (1988). Pathogenesis of dengue: challenges to molecular biology. Science *239*, 476–481. https://doi.org/10.1126/science.3277268.
8. Hadinegoro, S.R., Arredondo-García, J.L., Capeding, M.R., Deseda, C., Chotpitayasunondh, T., Dietze, R., Muhammad Ismail, H.I.H., Reynales, H., Limkittikul, K., Rivera-Medina, D.M., et al. (2015). Efficacy and Long-Term Safety of a Dengue Vaccine in Regions of Endemic Disease. N. Engl. J. Med. *373*, 1195–1206. https://doi.org/10.1056/NEJMoa1506223.
9. Halstead, S.B., Katzelnick, L.C., Russell, P.K., Markoff, L., Aguiar, M., Dans, L.R., and Dans, A.L. (2020). Ethics of a partially effective dengue vaccine: Lessons from the Philippines. Vaccine *38*, 5572–5576. https://doi.org/10.1016/j.vaccine.2020.06.079.
10. Halstead, S.B. (2018). Safety issues from a Phase 3 clinical trial of a live-attenuated chimeric yellow fever tetravalent dengue vaccine. Hum. Vaccines Immunother. *14*, 2158–2162. https://doi.org/10.1080/21645515.2018.1445448.
11. Shukla, R., Ramasamy, V., Shanmugam, R.K., Ahuja, R., and Khanna, N. (2020). Antibody-Dependent Enhancement: A Challenge for Developing a Safe Dengue Vaccine. Front. Cell. Infect. Microbiol. *10*, 572681. https://doi.org/10.3389/fcimb.2020.572681.
12. Halstead, S.B. (2017). Dengvaxia sensitizes seronegatives to vaccine enhanced disease regardless of age. Vaccine *35*, 6355–6358. https://doi.org/10.1016/j.vaccine.2017.09.089.
13. Pinheiro-Michelsen, J.R., Souza, R.d.S.O., Santana, I.V.R., da Silva, P.d.S., Mendez, E.C., Luiz, W.B., and Amorim, J.H. (2020). Anti-dengue Vaccines: From Development to Clinical Trials. Front. Immunol. *11*, 1252. https://doi.org/10.3389/fimmu.2020.01252.
14. Deng, S.Q., Yang, X., Wei, Y., Chen, J.T., Wang, X.J., and Peng, H.J. (2020). A Review on Dengue Vaccine Development. Vaccines *8*, 63. https://doi.org/10.3390/vaccines8010063.
15. Biswal, S., Mendez Galvan, J.F., Macias Parra, M., Galan-Herrera, J.F., Carrascal Rodriguez, M.B., Rodriguez Bueno, E.P., Brose, M., Rauscher, M., LeFevre, I., Wallace, D., et al. (2021). Immunogenicity and safety of a tetravalent dengue vaccine in dengue-naïve adolescents in Mexico City. Rev. Panam. Salud Públic *45*, e67. https://doi.org/10.26633/RPSP.2021.67.
16. Rivera, L., Biswal, S., Saez-Llorens, X., Reynales, H., Lopez-Medina, E., Borja-Tabora, C., Bravo, L., Sirivichayakul, C., Kosalaraksa, P., Martinez Vargas, L., et al. (2021). Three years efficacy and safety of Takeda's dengue vaccine candidate (TAK-003). Clin. Infect. Dis. *75*, 107–117. https://doi.org/10.1093/cid/ciab864.
17. Fourati, S., Cristescu, R., Loboda, A., Talla, A., Filali, A., Railkar, R., Schaeffer, A.K., Favre, D., Gagnon, D., Peretz, Y., et al. (2016). Pre-vaccination inflammation and B-cell signalling predict age-related hyporesponse to hepatitis B vaccination. Nat. Commun. *7*, 10369. https://doi.org/10.1038/ncomms10369.
18. Tsang, J.S., Schwartzberg, P.L., Kotliarov, Y., Biancotto, A., Xie, Z., Germain, R.N., Wang, E., Olnes, M.J., Narayanan, M., Golding, H., et al. (2014). Global analyses of human immune variation reveal baseline predictors of postvaccination responses. Cell *157*, 499–513. https://doi.org/10.1016/j.cell.2014.03.031.
19. Kotliarov, Y., Sparks, R., Martins, A.J., Mulè, M.P., Lu, Y., Goswami, M., Kardava, L., Banchereau, R., Pascual, V., Biancotto, A., et al. (2020). Broad immune activation underlies shared set point signatures for vaccine responsiveness in healthy individuals and disease activity in patients

with lupus. Nat. Med. *26*, 618–629. https://doi.org/10.1038/s41591-020-0769-8.

20. Parvandeh, S., Poland, G.A., Kennedy, R.B., and McKinney, B.A. (2019). Multi-Level Model to Predict Antibody Response to Influenza Vaccine Using Gene Expression Interaction Network Feature Selection. Microorganisms *7*, 79. https://doi.org/10.3390/microorganisms7030079.
21. Shen-Orr, S.S., and Furman, D. (2013). Variability in the immune system: of vaccine responses and immune states. Curr. Opin. Immunol. *25*, 542–547. https://doi.org/10.1016/j.coi.2013.07.009.
22. Tsang, J.S. (2015). Utilizing population variation, vaccination, and systems biology to study human immunology. Trends Immunol. *36*, 479–493. https://doi.org/10.1016/j.it.2015.06.005.
23. Kau, A.L., Ahern, P.P., Griffin, N.W., Goodman, A.L., and Gordon, J.I. (2011). Human nutrition, the gut microbiome and the immune system. Nature *474*, 327–336. https://doi.org/10.1038/nature10213.
24. Querec, T.D., Akondy, R.S., Lee, E.K., Cao, W., Nakaya, H.I., Teuwen, D., Pirani, A., Gernert, K., Deng, J., Marzolf, B., et al. (2009). Systems biology approach predicts immunogenicity of the yellow fever vaccine in humans. Nat. Immunol. *10*, 116–125. https://doi.org/10.1038/ni.1688.
25. Gaucher, D., Therrien, R., Kettaf, N., Angermann, B.R., Boucher, G., Filali-Mouhim, A., Moser, J.M., Mehta, R.S., Drake, D.R., Castro, E., et al. (2008). Yellow fever vaccine induces integrated multilineage and polyfunctional immune responses. J. Exp. Med. *205*, 3119–3131. https://doi.org/10.1084/jem.20082292.
26. Nakaya, H.I., Hagan, T., Duraisingham, S.S., Lee, E.K., Kwissa, M., Rouphael, N., Frasca, D., Gersten, M., Mehta, A.K., Gaujoux, R., et al. (2015). Systems Analysis of Immunity to Influenza Vaccination across Multiple Years and in Diverse Populations Reveals Shared Molecular Signatures. Immunity *43*, 1186–1198. https://doi.org/10.1016/j.immuni.2015.11.012.
27. Tomalka, J.A., Pelletier, A.N., Fourati, S., Latif, M.B., Sharma, A., Furr, K., Carlson, K., Lifton, M., Gonzalez, A., Wilkinson, P., et al. (2021). The transcription factor CREB1 is a mechanistic driver of immunogenicity and reduced HIV-1 acquisition following ALVAC vaccination. Nat. Immunol. *22*, 1294–1305. https://doi.org/10.1038/s41590-021-01026-9.
28. Pulendran, B. (2014). Systems vaccinology: probing humanity's diverse immune systems with vaccines. Proc. Natl. Acad. Sci. USA *111*, 12300–12306. https://doi.org/10.1073/pnas.1400476111.
29. Wimmers, F., and Pulendran, B. (2020). Emerging technologies for systems vaccinology - multi-omics integration and single-cell (epi)genomic profiling. Curr. Opin. Immunol. *65*, 57–64. https://doi.org/10.1016/j.coi.2020.05.001.
30. Kim, E.Y., Che, Y., Dean, H.J., Lorenzo-Redondo, R., Stewart, M., Keller, C.K., Whorf, D., Mills, D., Dulin, N.N., Kim, T., et al. (2022). Transcriptome-wide changes in gene expression, splicing, and lncRNAs in response to a live attenuated dengue virus vaccine. Cell Rep. *38*, 110341. https://doi.org/10.1016/j.celrep.2022.110341.
31. Nakaya, H.I., Wrammert, J., Lee, E.K., Racioppi, L., Marie-Kunze, S., Haining, W.N., Means, A.R., Kasturi, S.P., Khan, N., Li, G.M., et al. (2011). Systems biology of vaccination for seasonal influenza in humans. Nat. Immunol. *12*, 786–795. https://doi.org/10.1038/ni.2067.
32. Moncunill, G., Carnes, J., Chad Young, W., Carpp, L., De Rosa, S., Campo, J.J., Nhabomba, A., Mpina, M., Jairoce, C., Finak, G., et al. (2022). Transcriptional correlates of malaria in RTS,S/AS01-vaccinated African children: a matched case-control study. Elife *11*, e70393. https://doi.org/10.7554/eLife.70393.
33. Kallas, E.G., Precioso, A.R., Palacios, R., Thomé, B., Braga, P.E., Vanni, T., Campos, L.M.A., Ferrari, L., Mondini, G., da Graça Salomão, M., et al. (2020). Safety and immunogenicity of the tetravalent, live-attenuated dengue vaccine Butantan-DV in adults in Brazil: a two-step, double-blind, randomised placebo-controlled phase 2 trial. Lancet Infect. Dis. *20*, 839–850. https://doi.org/10.1016/S1473-3099(20)30023-2.
34. Kirkpatrick, B.D., Durbin, A.P., Pierce, K.K., Carmolli, M.P., Tibery, C.M., Grier, P.L., Hynes, N., Diehl, S.A., Elwood, D., Jarvis, A.P., et al. (2015). Robust and Balanced Immune Responses to All 4 Dengue Virus Serotypes Following Administration of a Single Dose of a Live Attenuated Tetravalent Dengue Vaccine to Healthy, Flavivirus-Naive Adults. J. Infect. Dis. *212*, 702–710. https://doi.org/10.1093/infdis/jiv082.
35. Kirkpatrick, B.D., Whitehead, S.S., Pierce, K.K., Tibery, C.M., Grier, P.L., Hynes, N.A., Larsson, C.J., Sabundayo, B.P., Talaat, K.R., Janiak, A., et al. (2016). The live attenuated dengue vaccine TV003 elicits complete protection against dengue in a human challenge model. Sci. Transl. Med. *8*, 330ra36. https://doi.org/10.1126/scitranslmed.aaf1517.
36. Dejnirattisai, W., Jumnainsong, A., Onsirisakul, N., Fitton, P., Vasanawathana, S., Limpitikul, W., Puttikhunt, C., Edwards, C., Duangchinda, T., Supasa, S., et al. (2010). Cross-reacting antibodies enhance dengue virus infection in humans. Science *328*, 745–748. https://doi.org/10.1126/science.1185181.
37. Schoggins, J.W., and Rice, C.M. (2011). Interferon-stimulated genes and their antiviral effector functions. Curr. Opin. Virol. *1*, 519–525. https://doi.org/10.1016/j.coviro.2011.10.008.
38. Au-Yeung, N., Mandhana, R., and Horvath, C.M. (2013). Transcriptional regulation by STAT1 and STAT2 in the interferon JAK-STAT pathway. JAK-STAT *2*, e23931. https://doi.org/10.4161/jkst.23931.
39. Mostafavi, S., Yoshida, H., Moodley, D., LeBoité, H., Rothamel, K., Raj, T., Ye, C.J., Chevrier, N., Zhang, S.Y., Feng, T., et al. (2016). Parsing the Interferon Transcriptional Network and Its Disease Associations. Cell *164*, 564–578. https://doi.org/10.1016/j.cell.2015.12.032.
40. Lazear, H.M., Schoggins, J.W., and Diamond, M.S. (2019). Shared and Distinct Functions of Type I and Type III Interferons. Immunity *50*, 907–923. https://doi.org/10.1016/j.immuni.2019.03.025.
41. Fredericksen, B.L., Keller, B.C., Fornek, J., Katze, M.G., and Gale, M., Jr. (2008). Establishment and maintenance of the innate antiviral response to West Nile Virus involves both RIG-I and MDA5 signaling through IPS-1. J. Virol. *82*, 609–616. https://doi.org/10.1128/JVI.01305-07.
42. Loo, Y.M., Fornek, J., Crochet, N., Bajwa, G., Perwitasari, O., Martinez-Sobrido, L., Akira, S., Gill, M.A., García-Sastre, A., Katze, M.G., et al. (2008). Distinct RIG-I and MDA5 signaling by RNA viruses in innate immunity. J. Virol. *82*, 335–345. https://doi.org/10.1128/JVI.01080-07.
43. Nasirudeen, A.M.A., Wong, H.H., Thien, P., Xu, S., Lam, K.P., and Liu, D.X. (2011). RIG-I, MDA5 and TLR3 synergistically play an important role in restriction of dengue virus infection. PLoS Neglected Trop. Dis. *5*, e926. https://doi.org/10.1371/journal.pntd.0000926.
44. Fourati, S., Tomalin, L., Mulè, M., Chawla, D., Gerritsen, B., Rychkov, D., Henrich, E., Miller, H., Hagan, T., Diray-Arce, J., et al. (2021). An innate immune activation state prior to vaccination predicts responsiveness to multiple vaccines. Preprint at bioRxiv. https://doi.org/10.1101/2021.09.26.461847.
45. Sullivan, N.L., Reuter-Monslow, M.A., Sei, J., Durr, E., Davis, C.W., Chang, C., McCausland, M., Wieland, A., Krah, D., Rouphael, N., et al. (2018). Breadth and Functionality of Varicella-Zoster Virus Glycoprotein-Specific Antibodies Identified after Zostavax Vaccination in Humans. J. Virol. *92*, e00269-18. https://doi.org/10.1128/JVI.00269-18.
46. Hagan, T., Cortese, M., Rouphael, N., Boudreau, C., Linde, C., Maddur, M.S., Das, J., Wang, H., Guthmiller, J., Zheng, N.Y., et al. (2019). Antibiotics-Driven Gut Microbiome Perturbation Alters Immunity to Vaccines in Humans. Cell *178*, 1313–1328.e13. https://doi.org/10.1016/j.cell.2019.08.010.
47. Pearce, E.L. (2021). Metabolism as a driver of immunity. Nat. Rev. Immunol. *21*, 618–619. https://doi.org/10.1038/s41577-021-00601-3.
48. Wammers, M., Schupp, A.K., Bode, J.G., Ehlting, C., Wolf, S., Deenen, R., Köhrer, K., Häussinger, D., and Graf, D. (2018). Reprogramming of pro-inflammatory human macrophages to an anti-inflammatory phenotype by bile acids. Sci. Rep. *8*, 255. https://doi.org/10.1038/s41598-017-18305-x.
49. Furusawa, Y., Obata, Y., Fukuda, S., Endo, T.A., Nakato, G., Takahashi, D., Nakanishi, Y., Uetake, C., Kato, K., Kato, T., et al. (2013). Commensal

microbe-derived butyrate induces the differentiation of colonic regulatory T cells. Nature *504*, 446–450. https://doi.org/10.1038/nature12721.

50. Hojjati, M.R., and Jiang, X.C. (2006). Rapid, specific, and sensitive measurements of plasma sphingomyelin and phosphatidylcholine. J. Lipid Res. *47*, 673–676. https://doi.org/10.1194/jlr.D500040-JLR200.
51. Ho, J., Cocolakis, E., Dumas, V.M., Posner, B.I., Laporte, S.A., and Lebrun, J.J. (2005). The G protein-coupled receptor kinase-2 is a TGFbeta-inducible antagonist of TGFbeta signal transduction. EMBO J. *24*, 3247–3258. https://doi.org/10.1038/sj.emboj.7600794.
52. Monaco, G., Lee, B., Xu, W., Mustafah, S., Hwang, Y.Y., Carré, C., Burdin, N., Visan, L., Ceccarelli, M., Poidinger, M., et al. (2019). RNA-Seq Signatures Normalized by mRNA Abundance Allow Absolute Deconvolution of Human Immune Cell Types. Cell Rep. *26*, 1627–1640.e7. https://doi.org/10.1016/j.celrep.2019.01.041.
53. Aran, D., Looney, A.P., Liu, L., Wu, E., Fong, V., Hsu, A., Chak, S., Naikawadi, R.P., Wolters, P.J., Abate, A.R., et al. (2019). Reference-based analysis of lung single-cell sequencing reveals a transitional profibrotic macrophage. Nat. Immunol. *20*, 163–172. https://doi.org/10.1038/s41590-018-0276-y.
54. Kawamata, Y., Fujii, R., Hosoya, M., Harada, M., Yoshida, H., Miwa, M., Fukusumi, S., Habata, Y., Itoh, T., Shintani, Y., et al. (2003). A G protein-coupled receptor responsive to bile acids. J. Biol. Chem. *278*, 9435–9440. https://doi.org/10.1074/jbc.M209706200.
55. Makishima, M., Lu, T.T., Xie, W., Whitfield, G.K., Domoto, H., Evans, R.M., Haussler, M.R., and Mangelsdorf, D.J. (2002). Vitamin D receptor as an intestinal bile acid sensor. Science *296*, 1313–1316. https://doi.org/10.1126/science.1070477.
56. Zenarruzabeitia, O., Vitallé, J., Eguizabal, C., Simhadri, V.R., and Borrego, F. (2015). The Biology and Disease Relevance of CD300a, an Inhibitory Receptor for Phosphatidylserine and Phosphatidylethanolamine. J. Immunol. *194*, 5053–5060. https://doi.org/10.4049/jimmunol.1500304.
57. Richard, A.S., Zhang, A., Park, S.J., Farzan, M., Zong, M., and Choe, H. (2015). Virion-associated phosphatidylethanolamine promotes TIM1-mediated infection by Ebola, dengue, and West Nile viruses. Proc. Natl. Acad. Sci. USA *112*, 14682–14687. https://doi.org/10.1073/pnas.1508095112.
58. Flores-Martin, J., Rena, V., Angeletti, S., Panzetta-Dutari, G.M., and Genti-Raimondi, S. (2013). The Lipid Transfer Protein StarD7: Structure, Function, and Regulation. Int. J. Mol. Sci. *14*, 6170–6186. https://doi.org/10.3390/ijms14036170.
59. Yang, L., Na, C.L., Luo, S., Wu, D., Hogan, S., Huang, T., and Weaver, T.E. (2017). The Phosphatidylcholine Transfer Protein Stard7 is Required for Mitochondrial and Epithelial Cell Homeostasis. Sci. Rep. *7*, 46416. https://doi.org/10.1038/srep46416.
60. Floris, A., Luo, J., Frank, J., Zhou, J., Orrù, S., Biancolella, M., Pucci, S., Orlandi, A., Campagna, P., Balzano, A., et al. (2019). Star-related lipid transfer protein 10 (STARD10): a novel key player in alcohol-induced breast cancer progression. J. Exp. Clin. Cancer Res. *38*, 4. https://doi.org/10.1186/s13046-018-1013-y.
61. Rohart, F., Gautier, B., Singh, A., and Lê Cao, K.A. (2017). mixOmics: An R package for 'omics feature selection and multiple data integration. PLoS Comput. Biol. *13*, e1005752. https://doi.org/10.1371/journal.pcbi.1005752.
62. Stockis, J., Colau, D., Coulie, P.G., and Lucas, S. (2009). Membrane protein GARP is a receptor for latent TGF-beta on the surface of activated human Treg. Eur. J. Immunol. *39*, 3315–3322. https://doi.org/10.1002/eji.200939684.
63. Wang, R., Zhu, J., Dong, X., Shi, M., Lu, C., and Springer, T.A. (2012). GARP regulates the bioavailability and activation of TGFβ. Mol. Biol. Cell *23*, 1129–1139. https://doi.org/10.1091/mbc.E11-12-1018.
64. Urcuqui-Inchima, S., Cabrera, J., and Haenni, A.L. (2017). Interplay between dengue virus and Toll-like receptors, RIG-I/MDA5 and microRNAs: Implications for pathogenesis. Antivir. Res. *147*, 47–57. https://doi.org/10.1016/j.antiviral.2017.09.017.
65. Kayesh, M.E.H., Kohara, M., and Tsukiyama-Kohara, K. (2021). Recent Insights Into the Molecular Mechanism of Toll-Like Receptor Response to Dengue Virus Infection. Front. Microbiol. *12*, 744233. https://doi.org/10.3389/fmicb.2021.744233.
66. Caielli, S., Veiga, D.T., Balasubramanian, P., Athale, S., Domic, B., Murat, E., Banchereau, R., Xu, Z., Chandra, M., Chung, C.H., et al. (2019). A CD4(+) T cell population expanded in lupus blood provides B cell help through interleukin-10 and succinate. Nat. Med. *25*, 75–81. https://doi.org/10.1038/s41591-018-0254-9.
67. Guthmiller, J.J., Graham, A.C., Zander, R.A., Pope, R.L., and Butler, N.S. (2017). Cutting Edge: IL-10 Is Essential for the Generation of Germinal Center B Cell Responses and Anti-Plasmodium Humoral Immunity. J. Immunol. *198*, 617–622. https://doi.org/10.4049/jimmunol.1601762.
68. Treede, I., Braun, A., Sparla, R., Kühnel, M., Giese, T., Turner, J.R., Anes, E., Kulaksiz, H., Füllekrug, J., Stremmel, W., et al. (2007). Anti-inflammatory effects of phosphatidylcholine. J. Biol. Chem. *282*, 27155–27164. https://doi.org/10.1074/jbc.M704408200.
69. Ariyama, H., Kono, N., Matsuda, S., Inoue, T., and Arai, H. (2010). Decrease in membrane phospholipid unsaturation induces unfolded protein response. J. Biol. Chem. *285*, 22027–22035. https://doi.org/10.1074/jbc.M110.126870.
70. Wang, S., Zhang, S., Liou, L.C., Ren, Q., Zhang, Z., Caldwell, G.A., Caldwell, K.A., and Witt, S.N. (2014). Phosphatidylethanolamine deficiency disrupts alpha-synuclein homeostasis in yeast and worm models of Parkinson disease. Proc. Natl. Acad. Sci. USA *111*, E3976–E3985. https://doi.org/10.1073/pnas.1411694111.
71. van der Veen, J.N., Kennelly, J.P., Wan, S., Vance, J.E., Vance, D.E., and Jacobs, R.L. (2017). The critical role of phosphatidylcholine and phosphatidylethanolamine metabolism in health and disease. Biochim. Biophys. Acta Biomembr. *1859*, 1558–1572. https://doi.org/10.1016/j.bbamem.2017.04.006.
72. Gay, I., Schwartz, Z., Sylvia, V.L., and Boyan, B.D. (2004). Lysophospholipid regulates release and activation of latent TGF-beta1 from chondrocyte extracellular matrix. Biochim. Biophys. Acta *1684*, 18–28. https://doi.org/10.1016/j.bbalip.2004.04.006.
73. Qing, J., Liu, C., Choy, L., Wu, R.Y., Pagano, J.S., and Derynck, R. (2004). Transforming growth factor beta/Smad3 signaling regulates IRF-7 function and transcriptional activation of the beta interferon promoter. Mol. Cell Biol. *24*, 1411–1425. https://doi.org/10.1128/MCB.24.3.1411-1425.2004.
74. Liu, J., Fei, Y., Zhou, T., Ji, H., Wu, J., Gu, X., Luo, Y., Zhu, J., Feng, M., Wan, P., et al. (2021). Bile Acids Impair Vaccine Response in Children With Biliary Atresia. Front. Immunol. *12*, 642546. https://doi.org/10.3389/fimmu.2021.642546.
75. Winkler, E.S., Shrihari, S., Hykes, B.L., Jr., Handley, S.A., Andhey, P.S., Huang, Y.J.S., Swain, A., Droit, L., Chebrolu, K.K., Mack, M., et al. (2020). The Intestinal Microbiome Restricts Alphavirus Infection and Dissemination through a Bile Acid-Type I IFN Signaling Axis. Cell *182*, 901–918.e18. https://doi.org/10.1016/j.cell.2020.06.029.
76. Hu, M.M., He, W.R., Gao, P., Yang, Q., He, K., Cao, L.B., Li, S., Feng, Y.Q., and Shu, H.B. (2019). Virus-induced accumulation of intracellular bile acids activates the TGR5-beta-arrestin-SRC axis to enable innate antiviral immunity. Cell Res. *29*, 193–205. https://doi.org/10.1038/s41422-018-0136-1.
77. Lagakos, W.S., Guan, X., Ho, S.Y., Sawicki, L.R., Corsico, B., Kodukula, S., Murota, K., Stark, R.E., and Storch, J. (2013). Liver fatty acid-binding protein binds monoacylglycerol in vitro and in mouse liver cytosol. J. Biol. Chem. *288*, 19805–19815. https://doi.org/10.1074/jbc.M113.473579.
78. Martin, G.G., Atshaves, B.P., McIntosh, A.L., Mackie, J.T., Kier, A.B., and Schroeder, F. (2005). Liver fatty-acid-binding protein (L-FABP) gene ablation alters liver bile acid metabolism in male mice. Biochem. J. *391*, 549–560. https://doi.org/10.1042/BJ20050296.

79. Wang, G., Bonkovsky, H.L., de Lemos, A., and Burczynski, F.J. (2015). Recent insights into the biological functions of liver fatty acid binding protein 1. J. Lipid Res. *56*, 2238–2247. https://doi.org/10.1194/jlr.R056705.

80. Hamers, A.A.J., Dinh, H.Q., Thomas, G.D., Marcovecchio, P., Blatchley, A., Nakao, C.S., Kim, C., McSkimming, C., Taylor, A.M., Nguyen, A.T., et al. (2019). Human Monocyte Heterogeneity as Revealed by High-Dimensional Mass Cytometry. Arterioscler. Thromb. Vasc. Biol. *39*, 25–36. https://doi.org/10.1161/ATVBAHA.118.311022.

81. Villani, A.C., Satija, R., Reynolds, G., Sarkizova, S., Shekhar, K., Fletcher, J., Griesbeck, M., Butler, A., Zheng, S., Lazo, S., et al. (2017). Single-cell RNA-seq reveals new types of human blood dendritic cells, monocytes, and progenitors. Science *356*, eaah4573. https://doi.org/10.1126/science.aah4573.

82. Pilling, D., Fan, T., Huang, D., Kaul, B., and Gomer, R.H. (2009). Identification of markers that distinguish monocyte-derived fibrocytes from monocytes, macrophages, and fibroblasts. PLoS One *4*, e7475. https://doi.org/10.1371/journal.pone.0007475.

83. Chistiakov, D.A., Killingsworth, M.C., Myasoedova, V.A., Orekhov, A.N., and Bobryshev, Y.V. (2017). CD68/macrosialin: not just a histochemical marker. Lab. Invest. *97*, 4–13. https://doi.org/10.1038/labinvest.2016.116.

84. Siegal, F.P., Kadowaki, N., Shodell, M., Fitzgerald-Bocarsly, P.A., Shah, K., Ho, S., Antonenko, S., and Liu, Y.J. (1999). The nature of the principal type 1 interferon-producing cells in human blood. Science *284*, 1835–1837. https://doi.org/10.1126/science.284.5421.1835.

85. Swiecki, M., and Colonna, M. (2015). The multifaceted biology of plasmacytoid dendritic cells. Nat. Rev. Immunol. *15*, 471–485. https://doi.org/10.1038/nri3865.

86. Rothman, A.L., and Ennis, F.A. (1999). Immunopathogenesis of Dengue hemorrhagic fever. Virology *257*, 1–6. https://doi.org/10.1006/viro.1999.9656.

87. Halstead, S.B., and O'Rourke, E.J. (1977). Dengue viruses and mononuclear phagocytes. I. Infection enhancement by non-neutralizing antibody. J. Exp. Med. *146*, 201–217. https://doi.org/10.1084/jem.146.1.201.

88. Xu, G., Salen, G., Shefer, S., Tint, G.S., Nguyen, L.B., Chen, T.S., and Greenblatt, D. (1999). Increasing dietary cholesterol induces different regulation of classic and alternative bile acid synthesis. J. Clin. Invest. *103*, 89–95. https://doi.org/10.1172/JCI4414.

89. Van Parys, A., Karlsson, T., Vinknes, K.J., Olsen, T., Øyen, J., Dierkes, J., Nygård, O., and Lysne, V. (2021). Food Sources Contributing to Intake of Choline and Individual Choline Forms in a Norwegian Cohort of Patients With Stable Angina Pectoris. Front. Nutr. *8*, 676026. https://doi.org/10.3389/fnut.2021.676026.

90. Stremmel, W., Merle, U., Zahn, A., Autschbach, F., Hinz, U., and Ehehalt, R. (2005). Retarded release phosphatidylcholine benefits patients with chronic active ulcerative colitis. Gut *54*, 966–971. https://doi.org/10.1136/gut.2004.052316.

91. Bolger, A.M., Lohse, M., and Usadel, B. (2014). Trimmomatic: a flexible trimmer for Illumina sequence data. Bioinformatics *30*, 2114–2120. https://doi.org/10.1093/bioinformatics/btu170.

92. Dobin, A., Davis, C.A., Schlesinger, F., Drenkow, J., Zaleski, C., Jha, S., Batut, P., Chaisson, M., and Gingeras, T.R. (2013). STAR: ultrafast universal RNA-seq aligner. Bioinformatics *29*, 15–21. https://doi.org/10.1093/bioinformatics/bts635.

93. Anders, S., Pyl, P.T., and Huber, W. (2015). HTSeq–a Python framework to work with high-throughput sequencing data. Bioinformatics *31*, 166–169. https://doi.org/10.1093/bioinformatics/btu638.

94. Wang, L., Wang, S., and Li, W. (2012). RSeQC: quality control of RNA-seq experiments. Bioinformatics *28*, 2184–2185. https://doi.org/10.1093/bioinformatics/bts356.

95. Love, M.I., Huber, W., and Anders, S. (2014). Moderated estimation of fold change and dispersion for RNA-seq data with DESeq2. Genome Biol. *15*, 550. https://doi.org/10.1186/s13059-014-0550-8.

96. Korotkevich, G., Sukhov, V., Budin, N., Shpak, B., Artyomov, M.N., and Sergushichev, A. (2021). Fast gene set enrichment analysis. Preprint at bioRxiv. https://doi.org/10.1101/060012.

97. Hanzelmann, S., Castelo, R., and Guinney, J. (2013). GSVA: gene set variation analysis for microarray and RNA-seq data. BMC Bioinf. *14*. https://doi.org/10.1186/1471-2105-14-7.

98. Levine, J.H., Simonds, E.F., Bendall, S.C., Davis, K.L., Amir, E.a.D., Tadmor, M.D., Litvin, O., Fienberg, H.G., Jager, A., Zunder, E.R., et al. (2015). Data-Driven Phenotypic Dissection of AML Reveals Progenitor-like Cells that Correlate with Prognosis. Cell *162*, 184–197. https://doi.org/10.1016/j.cell.2015.05.047.

99. Maaten, L.V.D. (2014). Accelerating t-SNE using tree-based algorithms. J. Mach. Learn. Res. *15*, 3221–3245.

100. Stuart, T., Butler, A., Hoffman, P., Hafemeister, C., Papalexi, E., Mauck, W.M., Hao, Y., Stoeckius, M., Smibert, P., and Satija, R. (2019). Comprehensive Integration of Single-Cell Data. Cell *177*, 1888–1902.e21. https://doi.org/10.1016/j.cell.2019.05.031.

101. Hao, Y., Hao, S., Andersen-Nissen, E., Mauck, W.M., 3rd, Zheng, S., Butler, A., Lee, M.J., Wilk, A.J., Darby, C., Zager, M., et al. (2021). Integrated analysis of multimodal single-cell data. Cell *184*, 3573–3587.e29. https://doi.org/10.1016/j.cell.2021.04.048.

102. Johnson, W.E., Li, C., and Rabinovic, A. (2007). Adjusting batch effects in microarray expression data using empirical Bayes methods. Biostatistics *8*, 118–127. https://doi.org/10.1093/biostatistics/kxj037.

103. Subramanian, A., Tamayo, P., Mootha, V.K., Mukherjee, S., Ebert, B.L., Gillette, M.A., Paulovich, A., Pomeroy, S.L., Golub, T.R., Lander, E.S., et al. (2005). Gene set enrichment analysis: a knowledge-based approach for interpreting genome-wide expression profiles. Proc. Natl. Acad. Sci. USA *102*, 15545–15550. https://doi.org/10.1073/pnas.0506580102.

104. Lachmann, A., Xu, H., Krishnan, J., Berger, S.I., Mazloom, A.R., and Ma'ayan, A. (2010). ChEA: transcription factor regulation inferred from integrating genome-wide ChIP-X experiments. Bioinformatics *26*, 2438–2444. https://doi.org/10.1093/bioinformatics/btq466.

105. Keenan, A.B., Torre, D., Lachmann, A., Leong, A.K., Wojciechowicz, M.L., Utti, V., Jagodnik, K.M., Kropiwnicki, E., Wang, Z., and Ma'ayan, A. (2019). ChEA3: transcription factor enrichment analysis by orthogonal omics integration. Nucleic Acids Res. *47*, W212–W224. https://doi.org/10.1093/nar/gkz446.

106. Rusinova, I., Forster, S., Yu, S., Kannan, A., Masse, M., Cumming, H., Chapman, R., and Hertzog, P.J. (2013). Interferome v2.0: an updated database of annotated interferon-regulated genes. Nucleic Acids Res. *41*, D1040–D1046. https://doi.org/10.1093/nar/gks1215.

107. Merico, D., Isserlin, R., and Bader, G.D. (2011). Visualizing gene-set enrichment results using the Cytoscape plug-in enrichment map. Methods Mol. Biol. *781*, 257–277. https://doi.org/10.1007/978-1-61779-276-2_12.

108. Frolkis, A., Knox, C., Lim, E., Jewison, T., Law, V., Hau, D.D., Liu, P., Gautam, B., Ly, S., Guo, A.C., et al. (2010). SMPDB: The Small Molecule Pathway Database. Nucleic Acids Res. *38*, D480–D487. https://doi.org/10.1093/nar/gkp1002.

STAR★METHODS

KEY RESOURCES TABLE

REAGENT or RESOURCE	SOURCE	IDENTIFIER
Antibodies		
CD19 (clone HIB19) PE/Dazzle 594	Biolegend	Cat#302252; RRID: AB_2563560
CD38 (clone HIT2) Alexa Fluor 700	Biolegend	Cat#303524; RRID: AB_2072781
CD10 (clone HI10a) APC-Cy7	Biolegend	Cat#312212; RRID: AB_2146550
IgD (clone IA6-2) PerCP-Cy7	Biolegend	Cat#348208; RRID: AB_10641706
CD20 (clone 2H7) FITC	Biolegend	Cat#302304; RRID: AB_314252
KI-67 (clone KI-67) BV421	Biolegend	Cat#350506; RRID: AB_2563860
BCL-2 (clone 100) Alexa Fluor 647	Biolegend	Cat#658706; RRID: AB_2563280
CD56 (clone HCD56) BV510	Biolegend	Cat#318340; RRID: AB_2561944
CD19 (clone HIB19) BV510	Biolegend	Cat#302242; Cat#302241; RRID: AB_2561668
CCR2 (clone K036C2) PerCP-Cy5.5	Biolegend	Cat#357204; RRID: AB_2562004
CD206 (clone 15-2) FITC	Biolegend	Cat#321104; RRID: AB_571905
CD11c (clone Bu15) PE-Cy7	Biolegend	Cat#337216; RRID: AB_2129790
CD124 (clone G077F6) PE	Biolegend	Cat#355004; RRID: AB_11219385
CD16 (clone 3G8) BV570	Biolegend	Cat#302036; RRID: AB_2632790
IgM (clone G20-127) PE-Cy7	BD Biosciences	Cat#551079; RRID: AB_394036
CD21 (clone B-ly4) PE	BD Biosciences	Cat#555422; RRID: AB_395816
IgG (clone G18-145) PE-Cy7	BD Biosciences	Cat#561298; RRID: AB_10611712
CD21 (clone B-ly4) PE	BD Biosciences	Cat#557327; RRID: AB_396641
CD3 (clone UCHT1) BUV737	BD Biosciences	Cat#564307; RRID: AB_2744390
HLA-DR (clone G46-6) BUV395	BD Biosciences	Cat#564040; RRID: AB_2738558
CD45 (clone HI30) BV786	BD Biosciences	Cat#563716; RRID: AB_2716864
CD163 (clone GHI/61) BV711	BD Biosciences	Cat#563889; RRID: AB_2738469
CD16 (clone 3G8) BV650	BD Biosciences	Cat#563692; RRID: AB_2869511
CD14 (clone M5E2) BV605	BD Biosciences	Cat#564054; RRID: AB_2687593
CD71 (clone M-A712) BV421	BD Biosciences	Cat#562995; RRID: AB_2737939
CD123 (clone 9F5) PE-Cy5	BD Biosciences	Cat#551065; RRID: AB_394029
CD80 (clone L307.4) APC-H7	BD Biosciences	Cat#561134; RRID: AB_10565974
CD11b (clone ICRF44) Alexa Fluor 700	BD Biosciences	Cat#557918; RRID: AB_396939
CD68 (Y1/82A) PE-CF594	BD Biosciences	Cat#564944; RRID: AB_2739021
CD3 (clone UCHT1) BV510	BD Biosciences	Cat#563109; RRID: AB_2732053
CD14 (clone M5E2) BUV805	BD Biosciences	Cat#612902; RRID: AB_2870189
Smad2(pS465/pS467)/Smad3(pS423/pS425) (clone O72-670) PE	BD Biosciences	Cat#562586; RRID: AB_11151915
CD68 (clone Y1/82A) BV421	BD Biosciences	Cat#564943; RRID: AB_2739020
CX3CR1 (clone 2A9-1) APC	Thermo Fisher	Cat#17-6099-42; RRID: AB_11149136
Biological samples		
Healthy adult PBMC samples before Butantan-DV/TV003 vaccination	Instituto Butantan	N/A
Healthy adult plasma samples from before Butantan-DV/TV003 vaccination	Instituto Butantan	N/A
Healthy adult PBMC	Emory University	N/A

(*Continued on next page*)

Continued

REAGENT or RESOURCE	SOURCE	IDENTIFIER
Chemicals, peptides, and recombinant proteins		
LIVE/DEAD Aqua Fixable Dead Cell Stain	Life Technologies	Cat#L34957
Nigericin	InvivoGen	Cat#tlrl-nig
Glycocholate	Sigma-Aldrich	Cat#G7132-5G
Lithocholic acid	Sigma-Aldrich	Cat#L6250-10G
L-α-Phosphatidylethanolamine	Sigma-Aldrich	Cat#P7943-25MG
L-α-Phosphatidylcholine	Sigma-Aldrich	Cat#P3556-25MG
R848 - Resiquimod	InvivoGen	Cat#tlrl-r848
Critical commercial assays		
Mesoscale U-PLEX assay (IFN-γ, IFN-β, IL-1β, IL-6, IL-8, IL-10, IL-17A, IL-18, TGF-β1, TGF-β2, TGF-β3 and TNFα)	Meso Scale Discovery	N/A
Cytofix/Cytoperm	BD Biosciences	Cat#554714
Foxp3/Transcription Factor Staining Buffer Set	Thermo Fisher	Cat#00-5523-00
FAM-Flica Caspase-1 (YVAD) Assay Kit	Immunochemistry Technologies	Cat#98
Easy Sep Humam Monocyte Enrichment Kit	Stem Cell Technologies	Cat#19059
Deposited data		
Raw and normalized data	This paper	GEO: GSE209760
CITE-Seq PBMC data at the prevaccination timepoint for an influenza vaccine	Kotliarov et al.[19]	https://doi.org/10.35092/yhjc.c.4753772
Tonic Interferon signatures	Mostafavi et al.[39]	https://www.ncbi.nlm.nih.gov/pmc/articles/PMC4743492/bin/NIHMS753214-supplement-4.xls; Table S1E
Software and algorithms		
Trimmomatic	Bolger et al.[91]	https://github.com/usadellab/Trimmomatic
STAR	Dobin et al.[92]	https://github.com/alexdobin/STAR
HTSeq	Anders et al.[93]	https://htseq.readthedocs.io/en/latest/index.html
RSeQC	Wang et al.[94]	https://rseqc.sourceforge.net/
DESeq2	Love et al.[95]	https://bioconductor.org/packages/release/bioc/html/DESeq2.html
R (version 4.2)	R Core Team	https://www.r-project.org/
pheatmap	Raivo Kolde	https://rdocumentation.org/packages/pheatmap/versions/1.0.12
fgsea	Korotkevich et al.[96]	https://bioconductor.org/packages/release/bioc/html/fgsea.html
GSVA	Hänzelmann et al.[97]	https://www.bioconductor.org/packages/release/bioc/html/GSVA.html
FlowJo	BD	https://www.flowjo.com/
RPhenograph	Levine et al.[98]	https://github.com/JinmiaoChenLab/Rphenograph
Rtsne	Van der Maaten et al.[99]	https://github.com/jkrijthe/Rtsne
mixOmics	Rohart et al. [61]	http://mixomics.org/
SingleR	Aran et al.	https://www.bioconductor.org/packages/release/bioc/html/SingleR.html
Seurat	Satija Lab[100,101]	https://satijalab.org/seurat/
celldex	Aran et al. [53]	https://bioconductor.org/packages/release/data/experiment/html/celldex.html
Cytoscape	Cytoscape Consortium	https://cytoscape.org
Original Code	This paper	https://doi.org/10.5281/zenodo.11193904

RESOURCE AVAILABILITY

Lead contact

Further information and requests for resources and reagents should be directed to and will be fulfilled by the lead contact, Rafick-Pierre Sékaly (janedoe@emory.edu).

Materials availability

This study did not generate new unique reagents

Data and code availability

- De-identified human bulk RNA Sequencing data (raw and normalized counts) have been deposited at GEO. They are publicly available as of the date of publication. Accession numbers are listed in the key resources table. This paper analyzes existing, publicly available data. These accession numbers for the datasets are listed in the key resources table.
- All original code has been deposited at Zenodo and is publicly available as of the date of publication. DOIs are listed in the key resources table.
- Any additional information required to reanalyze the data reported in this paper is available from the lead contact upon request.

EXPERIMENTAL MODEL AND STUDY PARTICIPANT DETAILS

Human participants

Thirty-five volunteers from the Phase 2 trial in Brazil were used in this study, based on their pre-vaccination seronegative status to all 4 DENV serotypes as measured by PRNT assay. Participants were recruited at the University of Sao Paulo, screened for major infections prior to vaccination, and given subcutaneously 10^3 plaque-forming units (PFU) of each viral serotype (1-4) of live attenuated tetravalent Butantan-DV/TV003. PBMCs and plasma were collected at Day 0, prior to vaccination, as depicted in Figure S1A nAb response to the vaccine was measured by PRNT assay at Day 28, Day 56 and Day 90. Participants were given a second immunization at Day 180. Further details about sex, age or other demographic factors are available in Table 1. Effect of age, sex, race/ethnicity were tested and no association was found with the vaccination outcome.

METHOD DETAILS

Flow cytometry staining

PBMCs from volunteers at day 0 were incubated with fluorochrome-conjugated antibodies for at least 15–20 min at 4°C or on ice, protected from light. For the B cell panel the following fluorochrome-conjugated anti-human antibodies were used: CD19 (HIB19) (Cat. Number: 302252), CD38 (HIT2) (Cat. Number: 303524), CD10 (HI10a) (Cat. Number: 312212), IgD (IA6-2) (Cat. Number: 348208), CD20 (2H7) (Cat. Number: 302304), KI-67 (KI-67) (Cat. Number: 350506), BCL-2 (Cat. Number: 658606), were all from BioLegend. IgM (G20-127) (Cat. Number: 551079), CD21 (B-ly4) (Cat. Number: 555422), IgG (G18-145) (Cat. Number: 561298), CD21 (B-ly4) (Cat. Number: 557327), were from BD Biosciences. LIVE/DEAD Fixable Dead Cell Stain (Life Technologies) (Cat. Number: L34957) was used to gate on live cells. Samples were acquired on a BD LSR II.

For the innate immune cell panel: CD3 (UCHT1) (Cat. Number: 564307), HLA-DR (G46-6) (Cat. Number: 564040), CD45 (HI30) (Cat. Number: 563716), CD163 (GHI/61) (Cat. Number: 563889), CD16 (3G8) (Cat. Number: 563692), CD14 (M5E2) (Cat. Number: 564054), CD71 (M-A712) (Cat. Number: 562995), CD123 (9F5) (Cat. Number: 551065), CD80 (L307.4) (Cat. Number: 561134), CD11b (ICRF44) (Cat. Number: 557918), CD68 (Y1/82A) (Cat. Number: 564944) were purchased from BD Biosciences. CD56 (HCD56) (Cat. Number: 318340), CD19 (HIB19) (Cat. Number: 302242), CCR2 (K036C2) (Cat. Number: 357204), CD206 (15-2) (Cat. Number: 321104), CD11c (Bu15) (Cat. Number: 337216) and CD124 (G077F6) (Cat. Number: 355004) were obtained from Biolegend. CX3CR1 (2A9-1) (Cat. Number: 17-6099-42) was obtained from eBioscience. Live/Dead Aqua (Cat. Number: L34957) was purchased from Invitrogen. Cells were first stained after centrifugation for 30 minutes for cell surface markers in Staining Buffer (PBS 1X + 2% FBS) and a viability dye (Live/Dead Aqua). Then, they were fixated and permeabilized with Cytofix/Cytoperm (BD Biosciences, Cat: 554714) for 20 minutes, followed by an intracellular staining with anti-CD68 in PermWash (5X) for 30 minutes. All centrifugations were done at 0-4 C. All incubations were done at ice-cold temperatures. Data was acquired on a BD Fortessa cytometer.

Metabolite stimulation

Monocyte Enrichment and culture. $CD14^+CD16^-$ Classical Monocytes were isolated by negative selection from PBMCs of healthy donors using the EasySep™ Human Monocyte Enrichment Kit (Cat# 19059, StemCell Technologies). Purity was assessed by Flow Cytometry (BD FACSymphony™ A5 Cell Analyzer) using a viability dye (LIVE/DEAD™ Fixable Aqua Dead Cell Stain Kit, Cat# L34957, Thermo Fisher), an anti-CD3 antibody (clone UCHT1, Cat# 563109, BD Biosciences), an anti-CD19 antibody (clone HIB19, Cat# 302241, Biolegend), an anti-CD14 antibody (clone M5E2, Cat# 612902, BD Biosciences) and anti-CD16 antibody (clone 3G8, Cat# 302036, Biolegend). Purities of enriched populations ranged between 80-95%.

For the assessment of production of TGF-β

500,000 $CD14^{+}CD16^{-}$ monocytes per well were either stimulated with PC (1 nM) and PE (1 nM), TGF−β (25 ng/ml, positive control), DMSO (vehicle control) or left unstimulated (negative control) for 30 min, 12 h, or 20 h in 96-well round bottom plates. PC and PE working concentrations were determined in a viability assay by co-culturing monocytes with five concentrations of the compounds for 24 h (Figure S7A). Supernatants were collected from these time points and frozen until time of use.

For the assessment of production of pro-inflammatory cytokines

500,000 $CD14^{+}CD16^{-}$ monocytes per well were used for this assay. First, monocytes were primed with LPS (1 μg/ml) for 4 h. Cells then were stimulated either with BA: GCA (100 nM) or LCA (50 nM), Nigericin (1 μM, positive control), DMSO (vehicle control) or left unstimulated (negative control) for 1, 6, 12 and 18 h in 96-well round bottom plates. BA working concentrations were determined in a viability assay by co-culturing monocytes with five concentrations of the compounds for 24 h (Figure S7B). Supernatants were collected from these time points and frozen until time of use.

For the assessment of inhibition of cytokines production after preconditioning with PC and PE

500,000 $CD14^{+}CD16^{-}$ monocytes per well were co-cultured with PC (1 nM), PE (1 nM), TGF-β (25 ng/ml, positive control), DMSO (vehicle control) or left unstimulated (negative control) for 12 and 20 h in 96-well round bottom plates. Cells then were stimulated with a of TLR7/8 agonist (R848, Resiquimod – Cat# tlrl-r848, InvivoGen) for 24 h. Supernatants were collected from all conditions.

Secreted cytokines in the supernatants were quantified using the Mesoscale Discovery platform/kits described below.

Cytokine assessment

U-PLEX assay (Meso Scale MULTI-ARRAY Technology) commercially available by Meso Scale Discovery was used for supernatants cytokine detection, according to manufacturer's instructions. A panel that included the following cytokines was used: IFN-γ, IFN-β, IL-1β, IL-6, IL-8, IL-10, IL-17A, IL-18, TGF-β1, TGF-β2, TGF-β3 and TNFα. Briefly, 25 μL of culture supernatants from each well was used in duplicates. Electrochemiluminescence was detected and measured by using MESO QuickPlex SQ 120 (Meso Scale Discovery Rockville, MD, United States). The results were extrapolated from the standard curve from each specific analyte and plotted in pg/mL using the DISCOVERY WORKBENCH v4.0 software (Meso Scale Discovery, Rockville, MD, United States).

Phosphorylation of SMAD2/3

After stimulation of 500,000 cells/well in serum-free media (AIM V – Cat 12055091, ThermoFisher) at the determined time points (30 minutes, 12 and 20 hours), plates were centrifuge and culture components were divided for downstream analysis. Serum-free was used to avoid contamination of cells with TGF-β in serum. Supernatants were collected for cytokine assessment and cells were stained using Transcription Factor Phospho (TFP) Buffer Set (Cat 563239, BD Biosciences). Briefly, after centrifugation, cells were fixed with 1 x TFP Fix/Perm Buffer for 40 minutes, then permeabilized with Perm Buffer III for 15 min and finally stained intracellularly with anti-Smad2(pS465/pS467)/Smad3 (pS423/pS425) (clone O72-670, Cat 562586, BD Biosciences), anti-CD68 (clone Y1/82A, Cat 564943, BD Biosciences) and a viability dye (LIVE/DEAD™ Fixable Blue Dead Cell Stain Kit, Cat L23105, Thermo Fisher) for 30 minutes. All incubations and centrifugation steps were performed a 4°C.

Active-caspase 1 staining

500,000 cells/well were plated and stained using the eBioscience™ Foxp3/Transcription Factor Staining Buffer Set (Cat# 00- 5523-00, Thermo Fisher). After priming with LPS (1 μg/ml) for 4 h, cells were stained with a viability dye (LIVE/DEAD™ Fixable Aqua Dead Cell Stain Kit, Cat L34957, Thermo Fisher) for 15 min at room temperature (RT); cells were stimulated at their respective times (15, 30 and 60 min) prior to resuspension with surface staining mix, composed of antibodies to CD3 (clone UCHT1, Cat 563109, BD Biosciences), CD19 (clone HIB19, Cat 302241, Biolegend), CD14 (clone M5E2, Cat 612902, BD Biosciences), and CD16 (clone 3G8, Cat 302036, Biolegend) and FAM-FLICA® Caspase-1 (YVAD) Assay Kit (Cat 98, ImmunoChemistry Technologies), for 20 min at RT; cells then were fixed with Fix/Perm buffer (provided by the kit) for 30 min at 4°C. Finally, cells were stained intracellularly with anti-CD68 (clone Y1/82A, Cat 564944, BD Biosciences) for 30 min at 4°C.

Cells were acquired on the BD FACSymphony™ A5 Cell Analyzer (Becton Dickinson, San Jose, CA) and analyzed with FlowJo v. 10.7.

QUANTIFICATION AND STATISTICAL ANALYSIS

Outcome definitions

nAb titer curves were integrated over time as a measure of serotype-specific response as an Area Under the Curve (AUC) approach using the logarithmic trapezoid rule (in base 10) between days 0 and 90. Breadth was calculated on the basis of detection/absence of nAb of all 4 serotypes (with a PRNT threshold of detection > 10) into High (all 4 serotypes) or low (<4 serotypes) at any time point between days 0-180. Calculation of peak responses (Table S4) was performed only on responder participants, by determining the maxima per serotype per participant.

Transcriptomic analysis

RNA was isolated using RNEasy micro-kit (QIAGEN) from frozen PBMC samples taken preimmunization, and the quality of the RNA was confirmed using an Agilent 2100 Bioanalyzer. Paired-end total RNA sequencing was performed at Beijing Genomics Institute (BGI) using a BGISeq500 sequencer for 30 million 100 bp reads. Samples were processed in 2 distinct sequencing runs, and

were thus batch corrected using ComBat[102]. Raw FASTQ files were processed at Case Western Reserve University with the Sekaly lab pipeline: After sequencing, reads are processed to remove Illumina adapters and low quality 3'-end bases using the Trimmomatic software[91], and then mapped to the reference human genome version GRCh38 using the RNA-seq optimized software STAR[92]. RSeQC was then used to asses strand-specificity of reads for all transcripts[94]. Transcript abundance was then estimated from unique mapped reads into raw counts using HTSeq[93]. R package DESeq2 (version 1.6.2) was then used to normalize read counts among samples and to identify differentially expressed genes between biological samples[95]. Serotype-specific AUC outcomes were used as continuous variables, or as discrete factors for Breadth. The batch effect was directly corrected for by including the batch in the design. A Wald test was used to evaluate the statistical relevance of the observed variations given its reproducibility between biological replicates, and a Benjamini-Hochberg correction for large number of measurements was applied to obtain adjusted p-values. Genes of interest were selected based statistical significance (nominal.p> 0.05), and Bayesian shrinkage estimation was applied to the fold change to estimate effect size more accurately. Hierarchical clustering with complete linkage was performed using Euclidean distance and displayed using the pheatmap R package.

Preranked Gene Set Enrichment Analysis (GSEA) was performed using fgsea[96] for each contrast and/or correlation against genesets extracted from the MSigDB (BROAD Institute)[103], CHEA[104,105] and Interferome databases[106]. The signed -log nominal p-value was used as a ranking metric. Genesets found to be significantly enriched associated with the breadth of the response were considered as differentially activated pathways. EnrichmentMap was then used to reduce pathway redundancy of enriched pathways by generating modules of overlapping genesets on the basis of shared genes using a Jaccard distance cutoff of <0.25[107]. Manual curation was used for naming the modules, on the basis of member geneset names and biological role of core genes.

GSVA (Gene Set Variation Analysis) R package[97] was then used to compute a sample-level geneset enrichment z-score for significant EnrichmentMap modules to be significantly enriched using GSEA, on the basis of the expression level of the core genes. Sample level z-scores were then used for correlation with other OMICs.

Metabolic profiling

Normalized expression values from Metabolon and CellCarta platforms were compared across Breadth groups using a Student's T-test. MSEA was used as an adaptation of GSEA on metabolite data by preranking the individual metabolites by their sign(t-value) * -log(p-value), and. compared to metabolic sets generated from the in-house Metabolon classifications or SMPDB (Small Molecule Pathway Database) pathways[108]. EnrichmentMap was then used to reduce pathway redundancy of enriched pathways by generating modules of metabolite sets on the basis of a Jaccard distance cutoff < 0.5[107]. The maximum nominal p-value across sets within a module was used as a surrogate metric of a module association to breadth. Sample level z-scores for EnrichmentMap module were generated on the core genes using GSVA. Those z-scores were then integrated with transcriptomic genesets selected z-scores to infer association across OMICs using Spearman correlation.

Unsupervised flow cytometry analysis

Individual FCS files generated by the BD FACS Diva software were imported into FlowJo Software for pregating on CD3-CD19-CD56- live cell cells (innate panel) or $CD19^{+}$ live cells (B cell panel). Selected events were then exported: from which an identical number of events per patient were then randomly subsampled into R.

For bioinformatic analysis of flow cytometry data, a custom script was made using tSNE for RPhenograph analysis was used to to generate clusters of cells based upon their marker expression[98], while clusters were projected on a tSNE dimension reduction of the data[99], allowing for visualization of high dimensional data in two dimensions and for events to be clustered based on similar expression of flow cytometry markers. This led to identification of innate and B cells subsets.

Frequency of events per samples was then computed per cluster and compared across breadth groups using a Welch's t-test for unequal variances. Median Fluorescence Intensity for each marker was computed for each cluster for comparison of expression profiles.

Single-cell transcriptomic analysis

Publicly available datasets of 10X healthy PBMC datasets were downloaded from a pre-vaccination influenza cohort[19] and imported as a Seurat object[100,101]. SingleR[53] was used to infer cell identities with the cluster method, combined with the Monaco reference dataset[52]. Cell identities were validated using both surface marker expression and transcriptional markers. GSVA was used on averaged gene expression per cell identity with the z-score method.

Integrative analysis

We leveraged a projection-based approach from the R package mixOmics[61] to characterize correlations between OMICs (RNA-Seq, metabolome, proteomics, FCM). A sparse least square regression (sPLS) was used across OMICs as pairwise comparisons: a pairwise projection on the same scale allowed to quantify the Pearson correlation coefficient between the features of the two data types was calculated. To assess the probability of obtaining a Pearson correlation equal to or greater than the one observed, we derived a p value based on the distribution of the Pearson correlations calculated between all pair of features of the two data types (*i.e.*, the statistical universe). Pearson correlations corresponding to a p value cutoff of 0.05 were considered significant.